



HAL
open science

Magnetostratigraphy of Cenozoic sediments from the Xining Basin: Tectonic implications for the northeastern Tibetan Plateau

Shuang Dai, Xiaomin Fang, Guillaume Dupont-Nivet, Chunhui Song, Junping Gao, Wout Krijgsman, Cor Langereis, Weilin Zhang

► **To cite this version:**

Shuang Dai, Xiaomin Fang, Guillaume Dupont-Nivet, Chunhui Song, Junping Gao, et al.. Magnetostratigraphy of Cenozoic sediments from the Xining Basin: Tectonic implications for the northeastern Tibetan Plateau. *Journal of Geophysical Research: Solid Earth*, 2006, 111 (B11), pp.B11102. 10.1029/2005JB004187 . hal-02957156

HAL Id: hal-02957156

<https://hal.science/hal-02957156>

Submitted on 5 Oct 2020

HAL is a multi-disciplinary open access archive for the deposit and dissemination of scientific research documents, whether they are published or not. The documents may come from teaching and research institutions in France or abroad, or from public or private research centers.

L'archive ouverte pluridisciplinaire **HAL**, est destinée au dépôt et à la diffusion de documents scientifiques de niveau recherche, publiés ou non, émanant des établissements d'enseignement et de recherche français ou étrangers, des laboratoires publics ou privés.

Magnetostratigraphy of Cenozoic sediments from the Xining Basin: Tectonic implications for the northeastern Tibetan Plateau

Shuang Dai,^{1,2} Xiaomin Fang,^{1,2} Guillaume Dupont-Nivet,³ Chunhui Song,¹
Junping Gao,¹ Wout Krijgsman,³ Cor Langereis,³ and Weilin Zhang¹

Received 25 November 2005; revised 15 May 2006; accepted 7 June 2006; published 11 November 2006.

[1] The Xining subbasin of the Longzhong basin holds the longest continuous Cenozoic stratigraphic record at the margin of the northeastern Tibetan Plateau. Despite a rich biostratigraphic content (including the Xiejia mammal fauna), the tectonic evolution of the basin is largely unconstrained. In this study we present stratigraphic, biostratigraphic, and magnetostratigraphic results that provide a basis for reconstructing the Cenozoic tectonic evolution of the Xining basin with respect to adjacent regions of the northeastern Tibetan Plateau. Magnetostratigraphic analysis from three red bed sections in the Xining basin indicates continuous deposition at low and nearly constant accumulation rates (average 2.2 cm/kyr) from 52.0 to 17.0 Ma. We interpret this result to indicate that no major regional tectonic event implying large sediment accumulation variations has affected the Xining basin deposition during this considerable time window. In detail, accumulation rate variations outline a three-stage evolution with 1.8 cm/kyr from 52.0 Ma to 34.5 Ma, 4.1 cm/kyr from 34.5 to 31.0 Ma, and 2.3 cm/kyr from 31.0 to 17.0 Ma. The second-order increase between 34.5 and 31.0 Ma can be interpreted to result from either a distal tectonic event or to be of climatic origin. Although the region was tectonically quiescent for much of the Cenozoic, tectonic activity occurred during basin initiation (or reactivation) at circa 55.0–52.5 Ma and during intense basin deformation after 17.0 Ma.

Citation: Dai, S., X. Fang, G. Dupont-Nivet, C. Song, J. Gao, W. Krijgsman, C. Langereis, and W. Zhang (2006), Magnetostratigraphy of Cenozoic sediments from the Xining Basin: Tectonic implications for the northeastern Tibetan Plateau, *J. Geophys. Res.*, *111*, B11102, doi:10.1029/2005JB004187.

1. Introduction

[2] Following Indo-Asia collision in Paleocene-Eocene time, deformation progressively propagated from the collision zone to the northern parts of the Tibetan Plateau either continuously [Houseman and England, 1996; Molnar *et al.*, 1993] or in stepwise fashion along lithospheric strike-slip faults [Metivier *et al.*, 1998; Meyer *et al.*, 1998; Tapponnier *et al.*, 2001]. The Tibetan Plateau shows a northeastward decreasing elevation generally interpreted to result from Plio-Quaternary deformation and uplift at the northeastern end of the deformation zone. However, recent geologic and thermochronologic constraints show that the northern Tibetan Plateau may have formed much earlier, e.g., in the middle Miocene [Fang *et al.*, 2004; George *et al.*, 2001] or

Eocene-Oligocene [Fang *et al.*, 2003; Gilder *et al.*, 2001; Jolivet *et al.*, 2002; Mock *et al.*, 1999; Sobel *et al.*, 2001; Wang *et al.*, 2003; Yin and Harrison, 2000; Yin *et al.*, 2002].

[3] Much of these studies have focused on dating the activity of the Altun Tagh Fault (ATF) and the Kunlun Fault (KF), two large sinistral strike-slip boundaries controlling deformation of the northeastern Tibetan Plateau. However, no consensus has been reached on the timing and displacement of these faults such that the age of deformation of the northern Tibetan Plateau is still unconstrained [Delville *et al.*, 2001; Li *et al.*, 2002; Meng *et al.*, 2001; Ritts and Biffi, 2000; Wang, 1997; Yin and Harrison, 2000; Yin *et al.*, 2002; Yue *et al.*, 2001b].

[4] Propagation of deformation along the ATF and KF also resulted in the formation of a series of parallel ranges typically separated by rhombic basins holding a sedimentary record of the formation and denudation of those ranges (Figure 1a) [Metivier *et al.*, 1998; Meyer *et al.*, 1998; Tapponnier *et al.*, 1990]. Dating sediments of these basin has proved an effective method to deciphering the history of deformation and uplift [Fang *et al.*, 2003, 2004, 2005; Horton *et al.*, 2004; Li, 1995; Li *et al.*, 1997; Meng *et al.*, 2001; Yin *et al.*, 2002; Yue *et al.*, 2004]. Amongst these basins, the Cenozoic Longzhong basin provides a unique

¹Key Laboratory of Western China's Environmental Systems, Ministry of Education of China and College of Resources and Environment, Lanzhou University, Gansu, China.

²Institute of Tibetan Plateau Research, Chinese Academy of Science, Beijing, China.

³Paleomagnetic Laboratory, Faculty of Science, Utrecht University, Utrecht, Netherlands.

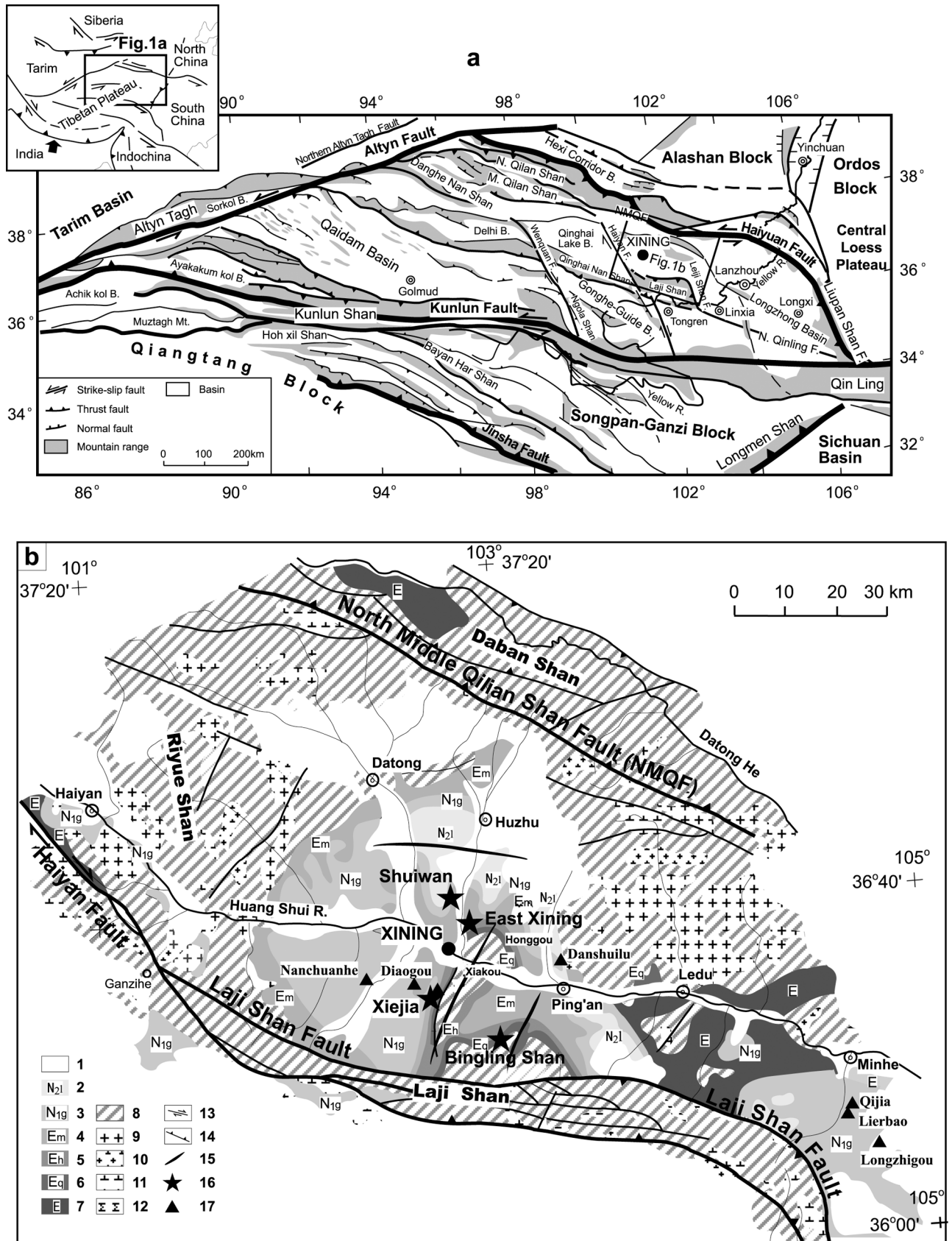


Figure 1

opportunity to reconstruct the deformation history. It is bounded by tectonic structures connected to the ATF and the KF and holds the most complete Cenozoic sedimentary record in the northeastern Tibetan Plateau. For these reasons it has been the locus of comparatively important geological investigations [Qinghai Bureau of Geology and Mineral Resources, 1985, 1991; Sun *et al.*, 1984; Yu *et al.*, 2003; Zhai and Cai, 1984]. An important biostratigraphic database including a rich record of fossil mammals of different evolutionary stages have been identified in this region [Flynn *et al.*, 1999; Qiu *et al.*, 2001, 1999]. Because of the absence of volcanic horizons datable using isotopic methods, magnetostratigraphy is the only mean to absolutely constraint the age deposits in this region. Magnetostratigraphy coupled with provenance, biostratigraphic and isotopic records and regional stratigraphy suggest basin activation (or reactivation) in Paleogene time followed by Miocene basin segmentation possibly associated with climate change [Dettman *et al.*, 2003; Fang *et al.*, 2003, 2005; Garziane *et al.*, 2005; Horton *et al.*, 2004; Qiu *et al.*, 2001]. Further investigations with improved age control on the Longzhong stratigraphy are needed to tightly correlate basin evolution with regional tectonics. Within the Longzhong basin, the best exposed, most continuous and longest Cenozoic stratigraphic record is preserved in the Xining subbasin. We present here a complete magnetostratigraphic record of the Cenozoic Xining basin successions.

2. Geological Background

[5] Located at the northeastern margin of the Tibetan Plateau, the Xining Basin is a subbasin in the western part of the larger Longzhong Basin [Zhai and Cai, 1984]. Cenozoic structures form the apparent boundaries of the exposed Longzhong Basin: the Qilian-Haiyuan faults to the north, the Liupan Shan fault to the east, the Haiyan-Laji Shan-Leiji Shan faults to the west and the North Qinling fault to the south (Figure 1a). The Longzhong Basin is generally divided into the Xining Basin to the west, the Lanzhou and Longxi subbasins to the east of and the Linxia subbasin to the southwest. Subbasins boundaries are defined by WNW-ESE trending structures extending from the Qilian Shan sinistral strike-slip faults system, and associated NW-SE trending dextral transpressional faults. Locally, the exposed Xining Basin is confined by the Daban Shan (Shan, mountain belt) to the north, the Laji Shan to the south, the Riyue Shan to the west, and a small upheaval to the east (Figure 1b). The exposed basin is bounded to the north and south by two sinistral transpressional fault systems (northern middle Qilian Shan Fault (NMQF) to the north and the Laji Shan Fault (LJF) system to the south). The present-day western boundary of the basin is a dextral transpressional system (the Haiyan Fault). The Cenozoic successions of the Xining basin are deformed by NNE directed structures in the southern half of the basin while the northern half is dominated by E-W trending structures.

[6] The particularly well-developed Cenozoic stratigraphy of the Longzhong basin is divided into the Paleogene Xining Group and the Neogene Guide Group [Zhai and Cai, 1984]. The Xining Group has a rich record of Paleogene ostracods, pollen and charophytes. In general, the Xining Group consists of a lower portion characterized by red-orange clastic sediments and an upper portion made of red mudstone with distinctive gypsiferous intercalations. The Guide Group generally consists of light brown to yellow mudstones with intercalated sandy and conglomeratic lenses that are abundant with fossil mammals. The contact between the Xining and the Guide Groups is generally described disconformable in the Longzhong basin but it is found conformable in the Xining (sub) basin [Qinghai Bureau of Geology and Mineral Resources, 1985, 1991]. The basement of the Xining basin consists of the Proterozoic gneisses and schists of the Huangyuan Group, Cambrian gray limestones and green basalts of the Maojiagou Group and Mesozoic sediments of Triassic, Middle Jurassic, Lower Cretaceous and Upper Cretaceous ages (Figure 1b) [Qinghai Bureau of Geology and Mineral Resources, 1991]. The Triassic consisting of purple and gray conglomerates, sandstones, fine sandstone and mudstone, is only marginally exposed in the Xining basin. The Middle Jurassic consists of conglomerates, sandstones and mudstones intercalated with coal beds. The Lower and Upper Cretaceous red beds of the Hekou and Minhe Group, respectively, consist of fine conglomerates, sandstones, and mudstones. These Jurassic-Cretaceous alluvial strata form a continuous package that is part of a larger preexisting basin referred to as the Xining-Minhe basin [Horton *et al.*, 2004]. In the Xining basin, Cenozoic successions are found concordantly lying on the alluvial Cretaceous Minhe Group or discordant on older basement rocks and start with reported sandstone and conglomeratic series indicating initiation or reactivation of the basin [Qinghai Bureau of Geology and Mineral Resources, 1985, 1991; Zhai and Cai, 1984]. On the basis of lithologic distinctions and fossil content, the continuously conformable >1000 m Cenozoic stratigraphy of playa to fluvio-lacustrine environments of the Xining basin is divided into the Xining and Guide Groups, further divided into six formations (and further subdivided into 16 members, see Table 1 for detailed lithologic descriptions and fossil content). Within the Xining Group, comparison of the rich ostracod, palynomorph and charophyte contents to that of other basins in China has yielded age correlation to (1) Paleocene to possibly lower Eocene for the Qijiachuan Formation, (2) Eocene for the Honggou Formation, and (3) Oligocene for the gypsiferous Mahalagou Formation [Hao, 1988; He *et al.*, 1988; Liu and Yang, 1999; Qinghai Bureau of Geology and Mineral Resources, 1991; Sun *et al.*, 1984; Yu *et al.*, 2001; Zhai and Cai, 1984; Wang *et al.*, 1990]. In addition, recently conducted palynological analyses confirm the Paleocene to Eocene designation for the Qijiachuan and Honggou formations [Horton *et al.*, 2004]. Within the Guide Group, in addition to pollen, ostracods and charophytes, Miocene

Figure 1. (a) Structural setting of the Xining basin (box) within the northeastern Tibetan Plateau (modified from Fang *et al.* [2005]). (b) Geological map of the Xining Basin. 1, Quaternary cover; 2, fanglomerate rocks; 3, Guide Group; 4, Mahalagou Formation; 5, Honggou Formation; 6, Qijiachuan formation; 7, undistinguished Paleogene rocks; 8, Precambrian-Mesozoic rocks; 9, granitic rocks; 10, granodioritic rocks; 11, dioritic rocks; 12, peridotitic rocks; 13, strike-slip faults; 14, thrust faults; 15, anticlinal axes; 16, section localities; 17, sites of fossil mammals.

Table 1. Xining Basin Stratigraphic Synthesis^a

Stratigraphy	Thickness, m	Lithologic Description	Fossils ^b
Linxia	>165	brown-yellow sandy mudstone with gray conglomerates	1: <i>Hipparion</i> cf. <i>Coelophyes</i> , <i>H.</i> sp., <i>Chleuastochoerus stehlini</i> , <i>Gazella</i> sp., <i>Cervidae</i> , <i>Giraforidae</i> , <i>Chilotherium</i>
Guide Group Xianshuihe N1xn2	>34	light brown-yellow calcareous mudstone with green and white marls	1: <i>Plesiodipus leei</i> , <i>Gomphotherium wimani</i> , ^{c,f} <i>G. connexus</i> , ^c <i>Elasmotherium</i> , ^c <i>Rhinocerotidae</i> indet., <i>Stephanocemas chinghaiensis</i> , ^d <i>Alloptox chinghaiensis</i> , ^e <i>Micromeryx</i> sp., ^f <i>Bunolistriodon minheensis</i> , ^f <i>Otoceros</i> (?) <i>noverca</i> , ^f 2: <i>Ilyocypris sublevis</i>
N1xn1	22–70	brown-yellow calcareous mudstone with grey sands and fine sandy mudstone	1: undistinguished from above; 2: <i>Maedlerisphaera chinensis</i>
Chetougou N1c2	77–163	brown-yellow calcareous mudstone with grey-white gypsiferous coarse sandstone	1: undistinguished from below; 2: <i>Limnocythere faceta</i> , <i>Eucypris magna</i> , <i>Eucypris flexilis</i> , <i>Cyprinotus xiningensis</i> , <i>Cylocypris xiningensis</i> ; 3: <i>Charites</i> cf. <i>chaidamuensis</i> , <i>Parvula</i> ; 4: <i>Quercoidites</i> , <i>Grammitaceae</i>
N1c1	3–82	red-yellow sandy calcareous mudstone with fine sandy mudstone; basal pebbly sandstone	1: <i>Megacricetodon sinensis</i> , ^{e,h} ? <i>Eumyarion</i> sp., <i>Heterosminthes orientalis</i> , <i>Palaeomeryx</i> sp., <i>Sinomicceros</i> , <i>Stephanocemas</i> sp., <i>Protolactaga tungrensis</i> , ^{g,h} <i>Rhinocerotidae</i> indet., ^h <i>Cervidae</i> indet., ^h 2: <i>Eucypris magna</i> ; 3: <i>Hornichara kasakstanica</i>
Xiejia N1x2	55–78	red-yellow sandy calcareous mudstone with fine sandy mudstone with pebbles	2: <i>Candoniella albicans</i> , <i>Potamocypris angulata</i> , <i>Ilyocypris evidens</i> , <i>Amplocypris daxiaensis</i> , <i>Cyprinotus geminiformis</i> , <i>Eucypris flexilis</i> , <i>Limnocythere faceta</i> ; 3: <i>Sphaerochara</i> cf. <i>granuliteri</i> ; 4: <i>Potamogeton</i> , <i>Quercoidites</i>
N1x1	23–200	red-yellow sandy mudstone with gypsiferous mudstone and pebbly sandstone	1: <i>Eucricetodon youngi</i> , <i>Sinolagomys pachygnathus</i> , <i>Plestiosminthus xiningensis</i> , <i>Pl. huangshuiensis</i> , <i>Pl. lajeensis</i> , <i>Tataromys suni</i> , <i>Tachyoryctoides kokonorensis</i> , <i>Rhinocerotidae Brachyotherium</i> sp., <i>Bovidae Otoceros</i> (?) <i>xiejiaensis</i> sp. nov., <i>Tataromys</i> sp., ⁱ <i>Leporidae</i> indet., <i>Synlagomis Pachygnathus</i> , <i>Aflantoxerus</i> , <i>Mustelidae</i> indet., <i>Diaceratherium</i> sp., <i>Cricetodontidae</i> indet., <i>Ctenodactylidae</i> indet.; 4: <i>Chenopodiipollis</i> , <i>Piceapollenites</i> , <i>Ulmipollenites</i>
Xining Group Mahalagou E3m3	146–253	Red sandy mudstone with gypsiferous (selenolite) sandy mudstone.	2: <i>Ilyocypris sublevis</i> ; <i>Ilyocypris bradyi</i> ; <i>Cyprinotus xiningensis</i> ; 3: <i>Hornichara kasakstanica</i> , <i>Maedlerisphaera globula</i> ; 4: <i>Chenopodiipollis</i> , <i>Piceapollenites</i>
E3m2	38–127	Red gypsiferous mudstone with greenwhite muddy gypsum (Mirabilite).	2: <i>Cyprinotus aff. qixianensis</i> Lee; 2: <i>Ilyocypris errabundis</i> , <i>Ilyocypris ellipsoides</i> ; 3: <i>Sphaerochara minheensis</i> , <i>Girogona qianjiangica</i> ; 4: <i>Ephedriptides</i> (D), <i>Meliaceoidites</i> , <i>Pinaceae</i>
E3m1	61–142	Green-white muddy gypsum (Mirabilite) with red gypsiferous mudstone.	2: <i>Potamocypris reiculata</i> , <i>Cyprinotus dongyaomiaozensis</i> ; 3: <i>Gyrogonia qianjiangica</i> , <i>Sphaerochara minheensis</i> ; 4: <i>Ephedriptides</i> (D), <i>Meliaceoidites</i>
Honggou E2h3	1–29	green-white laminated muddy gypsum	2: <i>Eucypris pengzhenensis</i> s; 4: <i>Ephedriptides</i> (E), <i>Quercoidites</i> , <i>TricolPoropollenites</i> , <i>Ulmipollenites</i>

Table 1. (continued)

Stratigraphy	Thickness, m	Lithologic Description	Fossils ^b
E2h2	50–131	red-orange fine sandy mudstone with green muddy gypsum	1: Rhynocerotidae indet.; 2: <i>Candona</i> sp.; 3: <i>Sphaerochara minheensis</i> , <i>Pseudolotochara pinnacle</i> ; 4: <i>Quercoidites</i> , <i>Celtis</i> , <i>Ioden</i>
E2h1	30–207	red sandstone with dolomite and green gypsiferous mudstone	2: <i>Limnocythere linguata</i> , <i>Ilyocypris gibba</i> ; 3: <i>Gyrogona qianjiangica</i> , <i>Pseudolotochara pinnacle</i> ; 4: <i>Ephedripites</i> , <i>Quercoidites</i> , <i>Celtis</i> , <i>Meliaceoidites</i>
QijiaChuan E1q3	23–107	mudstone with gypsiferous sandstone; basal “liver color” mudstone	4: Ephedripites (D., E.), <i>Polyodiataeisporites</i> , <i>Myrtaceoidites</i> , <i>Pterisporites</i> , <i>Quercoidites</i>
E1q2	24–48	mudstone with gypsiferous sandstone; upper dolomitic sandstone	4: Ephedripites (D., E.), <i>Parcisporites</i> , <i>Echitripites</i> , <i>Polyodiataeisporites</i> , <i>Myrtaceoidites</i>
E1q1	8–60	variegated mudstone with gypsiferous sandstone; basal gypsiferous pebbly sandstone	4: Ephedripites (D.), <i>Pinaceae</i> , <i>Proteacidites</i> , <i>Normapollis</i>

^aCompiled from Li and Qiu [1980], Li et al. [1981], Qinghai Bureau of Geology and Mineral Resources [1985, 1991], Qiu et al. [1981], Yu et al. [2001], and Zhai and Cai [1984]; thickness is stratigraphic thicknesses in meters.

^bFossils are 1, vertebrates; 2, ostracods; 3, charophytes (algae); 4, pollen.

^cDiagou, location of fossil mammal localities (Figure 1b).

^dLedu, location of fossil mammal localities (Figure 1b).

^eQijia, location of fossil mammal localities (Figure 1b).

^fLierbao, location of fossil mammal localities (Figure 1b).

^gLongzhigou, location of fossil mammal localities (Figure 1b).

^hDanshuile, location of fossil mammal localities (Figure 1b).

ⁱNianchanhe, location of fossil mammal localities (Figure 1b).

ages are supported by important vertebrate fossil content within (4) the early Miocene Xiejia Formation (including the Xiejia fauna uncovered at the location of our main magnetostratigraphic section), (5) the middle Miocene Chetougou Formation, and (6) the middle to late Miocene Xianshuihe Formation [Li and Qiu, 1980; Li et al., 1981; Qinghai Bureau of Geology and Mineral Resources, 1985, 1991; Qiu et al., 1999; Sun et al., 1984; Yu et al., 2001; Zhai and Cai, 1984]. Unconformably lying above the Guide Group successions, fanglomeratic rocks of the Linxia Group are reported to have yielded late Miocene to Pliocene fossils [Yu et al., 2001; Zhai and Cai, 1984].

3. Paleomagnetic Sampling and Analysis

[7] Three sections were chosen for sampling in the Xining basin. The main and longest section was sampled at Xiejia (36°31'N, 101°52'E, later referred as the Xiejia section; Figure 2) south of Xining City comprising continuous exposure of strata from the top of the Qijiachuan Formation to the base of the Xianshuihe Formation. A parallel section was sampled at Shuiwan (36°39'N, 101°52'E, later referred as the Shuiwan section) north of Xining city comprising strata from the base of the Mahalagou Formation to the base of the Xiejia Formation (see Figure 1b for location and Figure 3 for sections). Different bedding attitudes within the Xiejia section provide the opportunity to perform a fold test. The change in bedding tilt at the Xiejia section occurs coincidentally between the top of the Mahalagou Formation and the base of the Xiejia Formation. Note that this change of bedding attitude is related to a monoclinical structure acquired in late Neogene time as evidenced by the continuous thickness of beds that can be traced across the cylindrical fold (i.e., they do not pinch out and are not truncated as would be expected for an angular unconformity). A change in bedding attitude occurs at the Shuiwan section at a stratigraphic level higher than the sampled section within the Chetougou Formation. Stratigraphic correlation between these two sections is straightforward due to the occurrence of distinctive gypsiferous marker beds within the Mahalagou and Honggou formations easily traceable across the ~15 km separating these sections. The lower member of Qijiachuan Formation forming the base of the Xining group was sampled at the Bingling Shan section (36°26'N, 102°00'E). A previously published magnetostratigraphy of the Honggou Formation at the East Xining section located between the Xiejia and Shuiwan sections (36°35'N, 101°53'E) provides an additional parallel section for result comparison [Horton et al., 2004]. Hand sampling at 1–2 m thick stratigraphic intervals was performed along a 1–2 m deep trench in the Xiejia and Bingling Shan sections. At levels where clear characteristic remanence directions could not be isolated in the laboratory a second set of samples were collected by digging deeper pits in the trench. A third set of samples were later taken at 0.25 meter thick intervals in parts of the section where magnetic polarity zones were not clearly defined. A total of 1649 oriented block samples were collected from the Xiejia and Bingling Shan sections. These block samples were further cut into 2 × 2 × 2 cm³ cubic specimen in the laboratory, forming three sets of specimen. In the parallel Shuiwan section, sampling was performed using a portable

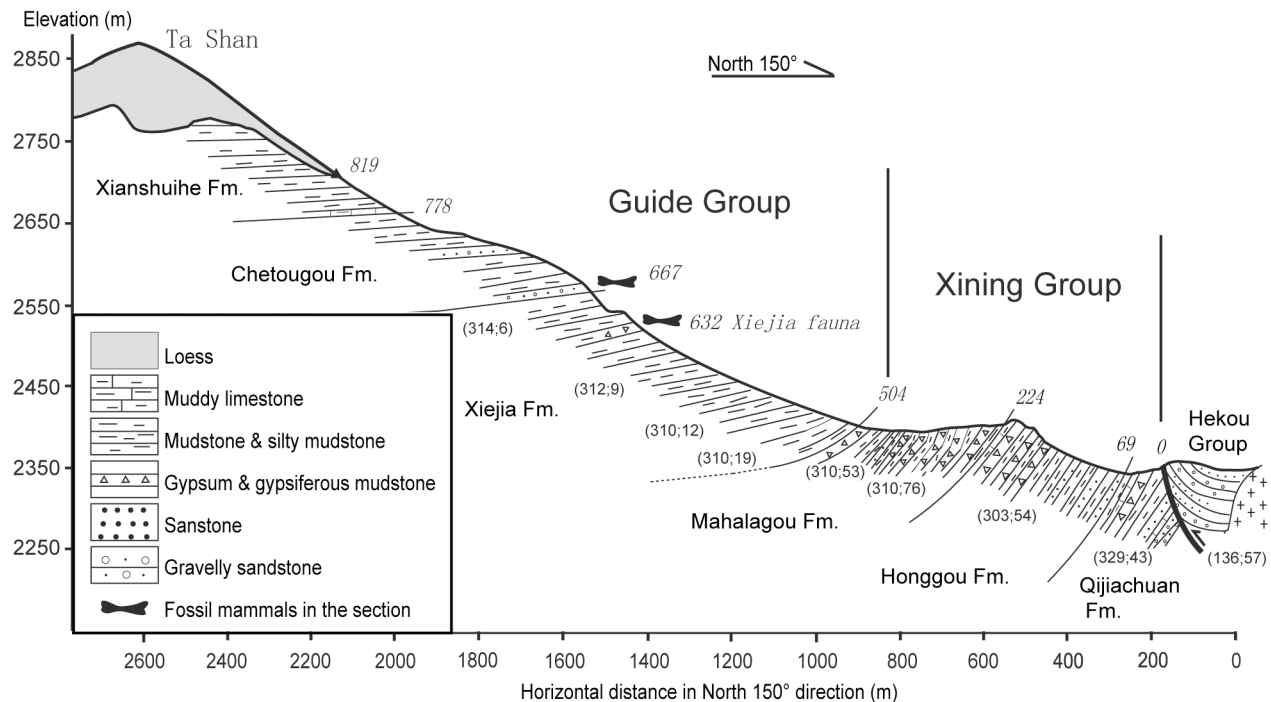


Figure 2. Cross section at Xiejia showing the measured stratigraphic successions of the Xining and Guide Groups (see Figure 1b for location). Measured stratigraphic thicknesses are indicated in meters by italic numbers. Measured bedding attitudes are indicated by numbers in parentheses (azimuth of strike is from north; dip in degrees is to the right of strike direction).

and gasoline-powered drill. Two to four samples were collected at an average stratigraphic spacing of 2 m except in the top 50 m of the section sampled at ~5 m thick intervals. A total of 84 levels were collected in the Shuiwan section.

[8] All the specimens were thermally demagnetized in 12 to 20 steps at 10–50°C intervals between 50°C and 690°C. Remanent magnetizations and directions of one set of the specimen from the Xiejia section were measured on a 2G cryogenic magnetometer in a magnetically shielded room in the Institute of Geology and Geophysics of Chinese Academy of Science. The second set of the specimen from the Xiejia section, and samples from Shuiwan and Bingling Shan sections were measured on the 2G cryogenic magnetometer in the Paleomagnetism Laboratory of the Utrecht University, the Netherlands. The third set of samples from the Xiejia section was measured on the 2G cryogenic magnetometer in the shielded room of the Paleomagnetic Laboratory at the Lanzhou University, China. At these three laboratories, similar magnetic behavior is obtained. Except for the Bingling Shan section where a majority of samples yielded no interpretable characteristic remanent magnetization (ChRM) directions, most samples have strong remanent magnetizations with clear isolation of ChRM directions (Figure 4). Two components are generally distinguished based on their contrasting directions and intensities. A low-temperature component (LTC) in roughly normal polarity direction is generally removed between 50°C and 200°C but sometimes up to 300–450°C. This LTC is interpreted as removal of a secondary remanent magnetization. A high-temperature component (HTC) in both normal and polarity directions shows generally linear decay from 200°C upon

reaching noise level at 650–690°C. For most samples throughout the stratigraphy, a minor remanence drop at ~580°C suggests that the HTC-carrying minerals are a combination of magnetite and mostly hematite. For a small number of samples, demagnetization behavior shows low initial remanence with unstable directions that do not decay toward the origin. From this last type, no ChRM directions could be estimated. To further assess the origin of the ChRMs isolated by thermal demagnetization, a variety of rock magnetic measurements were undertaken. Twenty-three representative samples were selected for IRM acquisition and back field measurements, thermal demagnetization of three-axis IRM components measurements in the Paleomagnetism Laboratory of Lanzhou University and hysteresis loop measurements in Paleomagnetic Laboratory of Utrecht University. The IRM acquisition was obtained for X axis of a cubic sample on a ASC IM-10–30 pulse magnetizer by stepwise application of magnetic fields until 2.5 T, and measured on a Agico JR5-A spinner magnetometer. Back field measurements of the samples were also carried out on the spinner magnetometer until remanence went to negative values. Then fields 2.5, 0.5 and 0.12 T were applied to X, Y, Z axes of the samples followed with systematic thermal demagnetizations at 10–50°C intervals between 50°C and 700°C and measured as well on the JR5-A spinner magnetometer following the procedure of Lowrie [1990]. On the basis of these experiments, two types of magnetic behaviors are distinguished. First type behaviors are dominant in investigated samples throughout the stratigraphy. They show gradual slow rise of IRM acquisition until reaching moderate Hcrs at ~400 mT (Figures 5a and 5b) and thermal demagnetization of IRM with distinct drops at ~150°C, linear

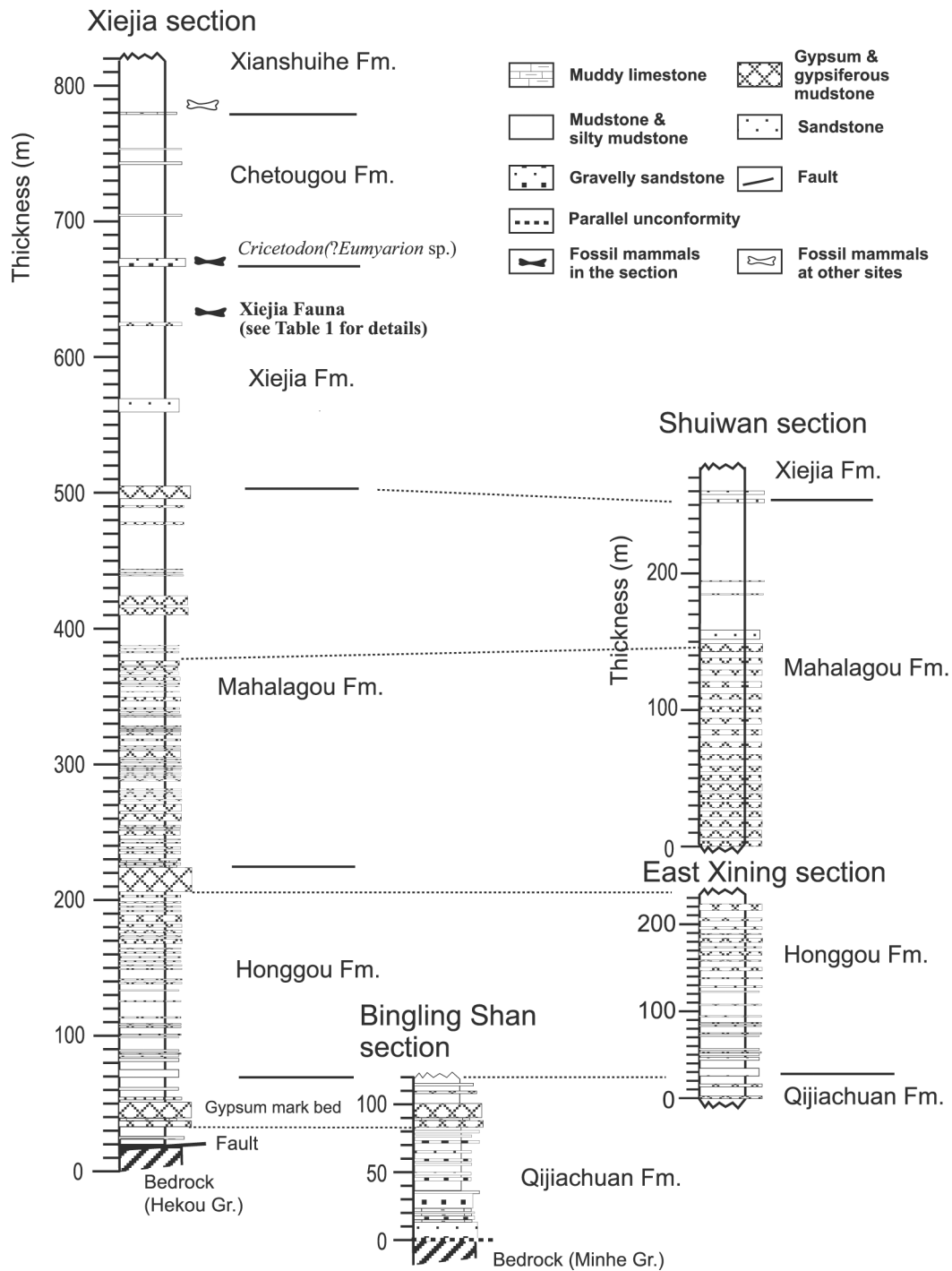


Figure 3. Stratigraphy, lithology, and correlation of the three sampled sections in the Xining Basin.

decay of all IRMs components down to 550–600°C and a final drop to 0 of the hard IRM at ~650–700°C. The first drop at ~150°C is interpreted to result from the presence of goethite and may explain the most part of the secondary remanent magnetization. Linear decay of IRM components down to 550–600°C can be interpreted to result from the presence of magnetite and the final drop at 650–700°C along with the high-coercivity IRM acquisition spectrum clearly indicates an important contribution of hematite. Second type behaviors were found in some investigated samples from Guide group in the upper part

of the stratigraphy. Similarly to type one samples, type two samples have a large contribution of hematite shown by unsaturated IRM at 2.5 T and a final drop to 0 of the hard IRM at ~650–700°C. Type two samples differ from type one samples however by showing a very sharp rise of IRM acquisition before 100–200 mT and a significant (over 50% of total IRM) soft component mostly demagnetized after a drop at 300–400°C. We speculate that this atypical behavior may indicate oxidation of primary minerals such as partial maghemitization of magnetite typically characterized by coercivity and thermal spectrum

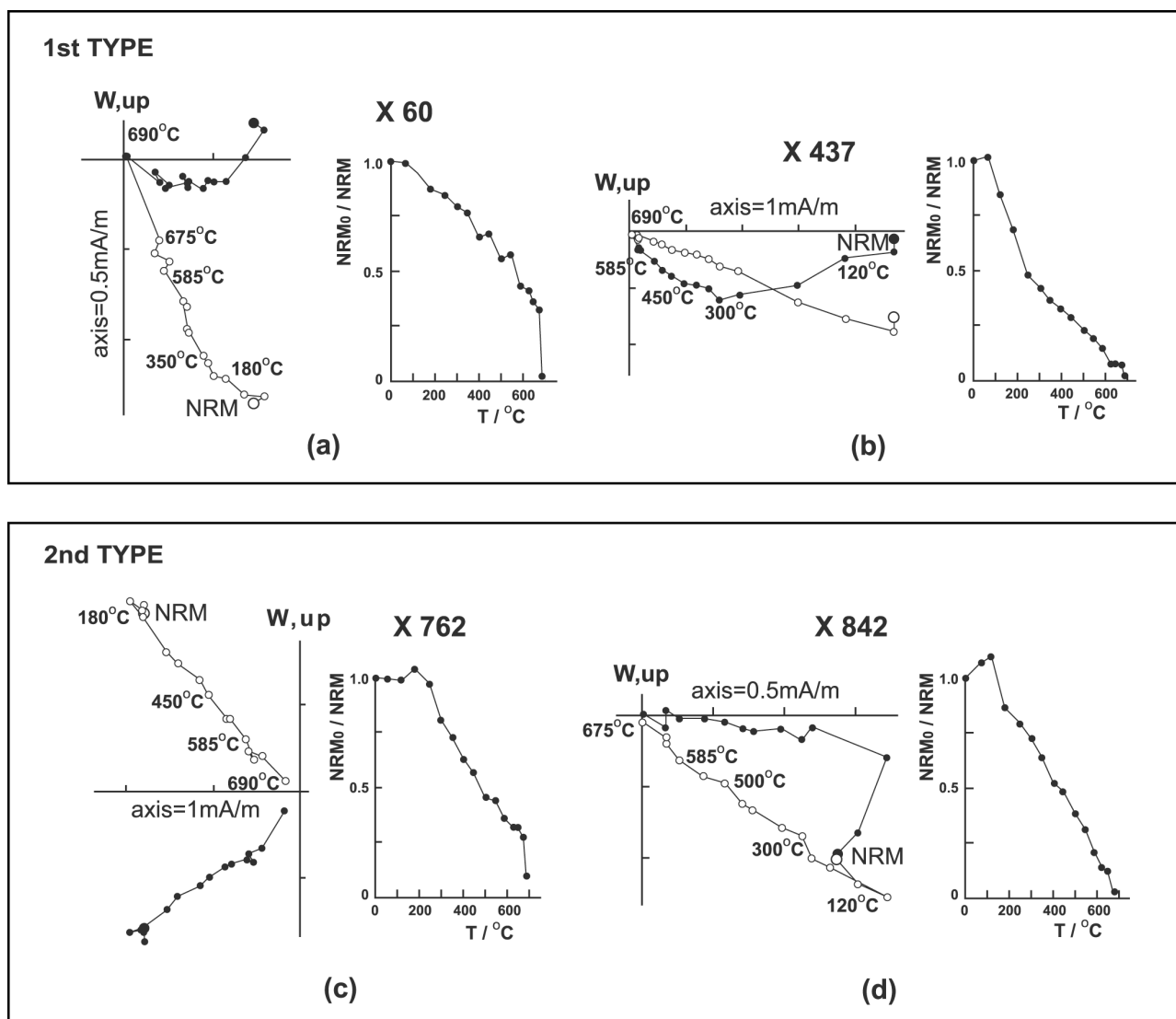


Figure 4. Representative thermal orthogonal demagnetization diagram and temperature decay of NRM for samples from the Xiejia section. Solid (open) circles represent horizontal (vertical) projections.

more compatible with our results than higher coercivity pigmentary hematite [de Boer and Dekkers, 1996; Tauxe and Badgley, 1988]. Interestingly, the distinction between the two behavioral types is not readily discernable from looking at thermal demagnetization of NRM only (Figure 4). In any case, this low-coercivity component observed in a few samples has a direction and polarity (normal and reverse) similar to the high-coercivity/high-temperature ChRM component carried by hematite and therefore does not interfere in the polarity determination of importance for this study. On the basis of our experiments, we cannot distinguish whether the hematite is purely depositional or acquired slightly after deposition during rubification. The ChRM directions of the samples were determined using principal component analysis on the HTC only (above 450°C) and were rejected for Maximum Angular Deviation (MAD) >30° [Kirschvink, 1980]. As previously stated, most levels from the Bingling Shan section yielded erratic demagnetization directions with low initial NRM intensities precluding magnetostratigraphic analysis for the Bingling Shan section. Finally, interpretable

ChRM directions could be obtained from 760 and 75 magnetostratigraphic levels from the Xiejia and Shuiwan sections, respectively (auxiliary material Tables S1 and S2).¹ Virtual geomagnetic polarity (VGP) latitudes were calculated from these ChRM directions. Only VGP latitudes above 45° are used for polarity determination while VGP latitudes below 45° were systematically discarded. The interpretable ChRM vectors cluster in antipodal direction after correction of bedding tilt (Figures 6a–6f) and pass the parametric fold and reversals tests [Tauxe, 1998] (Figures 6h and 6i) strongly suggesting a primary origin of the HTC ChRM.

4. Magnetostratigraphic Analysis

[9] The obtained magnetostratigraphic record indicates a large number of polarity zones within 800 meter of sampled

¹Auxiliary materials are available at <ftp://ftp.agu.org/apend/jb/2005jb004187>.

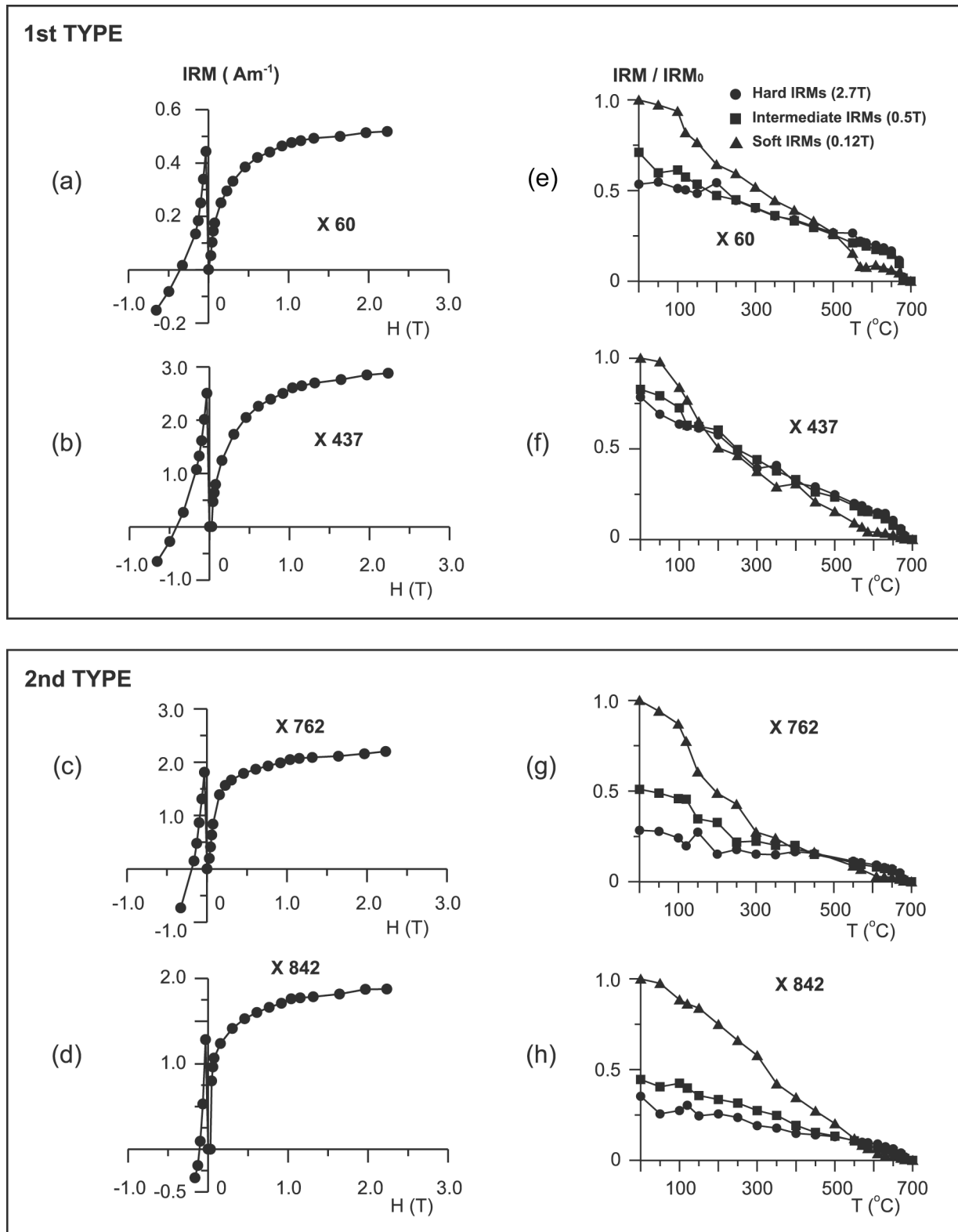


Figure 5. (a–d) IRM acquisition with back field measurement and (e–h) thermal demagnetization of three axis IRM components for selected samples from the Xiejia section.

stratigraphy (23 normal polarity zones N1–N23 and 24 reversed zones R0–R23 from the Xiejia section; four normal zones N1–N4 and four reversed zones R0–R3 from Shuiwan section). In addition, a total of 15 questionable

polarity zones are defined by one sample only (indicated by half length symbols on Figure 7), which represents stratigraphic intervals as low as 0.5 m in the Xiejia section. A few of these small polarity zones may be attributed to

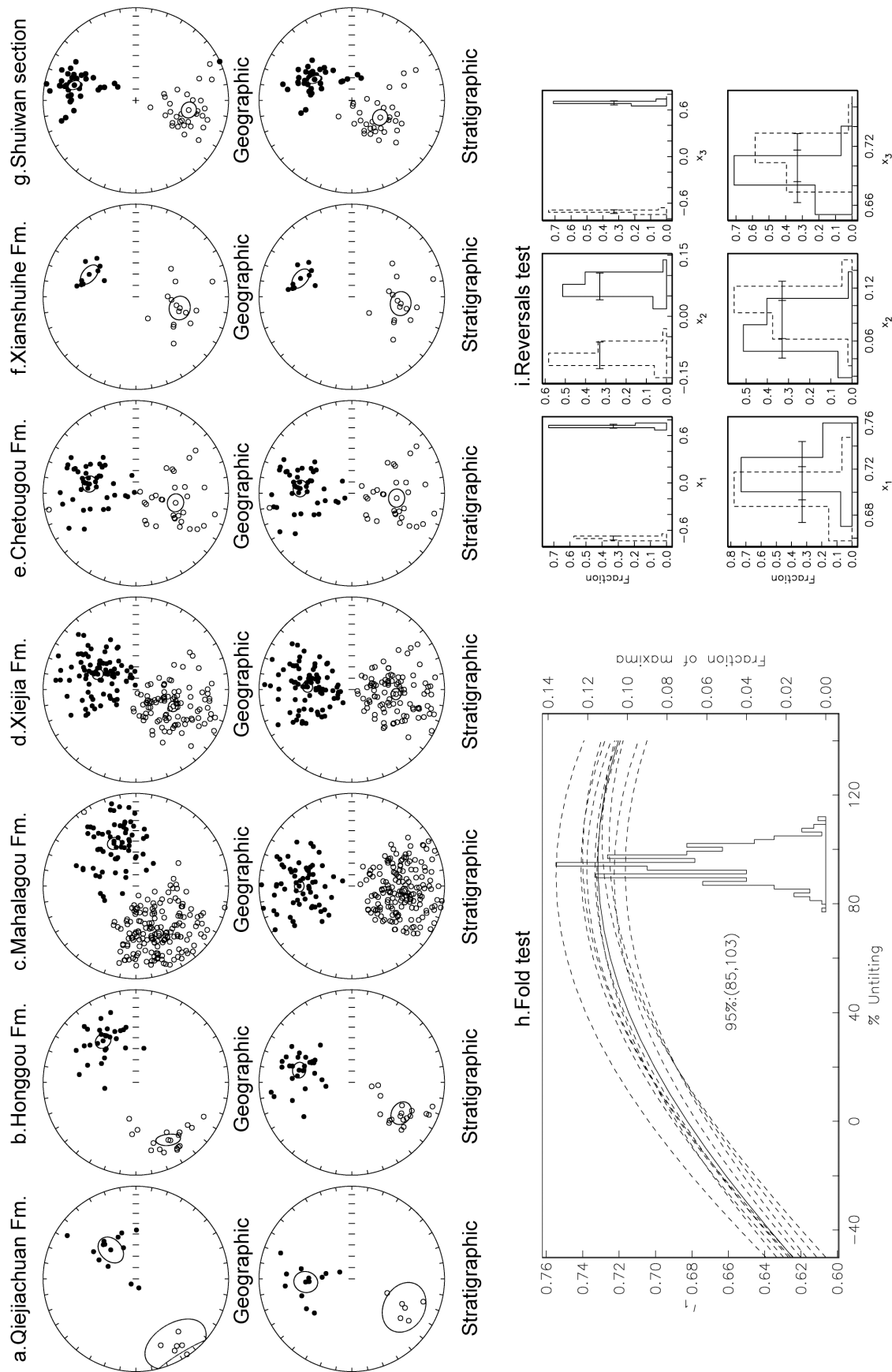


Figure 6. Equal-area projections of characteristic remanent magnetization (ChRM) directions in geographic (before tilt correction) and stratigraphic (after tilt correction) coordinates by formation (a–f) for the Xiejia (XJ) section and (g) for the entire Shuiwan (SW) section. Downward (upward) directions are shown as solid (open) circles. ChRM directions have (h) positive fold test and (i) reversals test [Tauxe, 1998].

unidentified secondary magnetization component, delayed acquisition near reversal boundaries or occasional sampling orientation errors. However, some of these may also represent a primary recording of the paleomagnetic field since a recent overprint would be simply detected through bedding tilt correction and a few of these short polarity intervals can be correlated across the parallel sections (for example R2 of Shuiwan to the reversed interval within N16 of Xiejia or N15 of Xiejia to the normal interval within R1 of Shuiwan). In any case, the high reversal rates in the comparatively low stratigraphic thickness represented by the sampled sections (hundreds of meters) points to low continuous accumulation rates during a large time span. This is corroborated by the following facts: (1) the Paleocene-Eocene to Miocene fossil content and the apparent continuity of the lacustrine distal stratigraphy with accumulation rates on the order of 1–10 cm/kyr and (2) comparably low accumulation rates are recorded at other sections from the Longzhong basin in the same age range [Fang *et al.*, 2003; Qiu *et al.*, 2001; Yue *et al.*, 2001a]. These observations together point already to the first-order outcome of this study: the Longzhong basin located at the margin of the present-day Tibetan Plateau is characterized by low sediment accumulation rates during most of Cenozoic time. Because of these low accumulation rates, insufficient sampling resolution, minor diastems (gaps in the sedimentary record) and small variations of the sediment accumulation rates may explain that the recorded pattern of polarity zones differs from the pattern expected from the geomagnetic polarity timescale of *Cande and Kent* [1995] (later referred as the GPTS). As a result, correlation to the GPTS is not unique (Figure 8). However, the absence of angular or erosional unconformity and the similarity of sedimentary facies throughout the sections allow the important assumptions that no major hiatus or drastic accumulation rate variations have affected the stratigraphy. On the basis of these assumptions, we propose a correlation of recorded polarity zones to the GPTS that can be rationally justified as follows.

4.1. Correlation to the GPTS

[10] As a starting point, we use the most distinctive pattern in both parallel sections lying in the Mahalagou Formation where two strikingly long reversed zones (R0 and R1 at Shuiwan; R14 and R15 at Xiejia) are separated by a shorter normal interval (N1 at Shuiwan and N15 at Xiejia). In agreement with the late Paleogene fossil content of the Mahalagou Formation the only reasonable fit to this polarity pattern is provided by the C12r-C13n-C13r sequence of the GPTS. Correlating the long observed reversed intervals higher on the GPTS where the reversal rate is high would imply unrealistic increase of accumulation rates (at least one order of magnitude higher ~ 50 – 100 cm/kyr) fortuitously during the duration of these chrons. Correlation below would require these long reversed chrons to be expressed higher in the section where recorded polarity zones are short, ultimately implying a unrealistic decrease in accumulation rates (at least one order of magnitude lower 0.1 – 0.01 cm/kyr). Such large variations in accumulation rates would likely be indicated by facies variations (e.g., conglomerates, disconformity or unconformity) that are not observed. Additional support of our correlation is that a similar pattern of long reversals has been recorded in the

stratigraphic equivalent of the Mahalagou Formation in the Lanzhou basin (the upper part of the Yehucheng Formation) which led [Yue *et al.*, 2001a, 2001b] and [Qiu *et al.*, 2001] to the same correlation. Furthermore, below the above mentioned distinctive reversal sequence, three dominantly normal intervals recorded in the lower part of the Mahalagou Formation both at Shuiwan (N2 to N4) and Xiejia (N16 to N18) provide a reasonable correlation with C15n to C18n of the GPTS. Further below, the lowermost part of the Mahalagou Formation and the upper member of the Honggou Formation were sampled at Xiejia section only but a parallel magnetostratigraphic record of the lower and middle members of the Honggou was previously acquired at the East Xining section [Horton *et al.*, 2004]. In agreement with the Eocene fossil content of the Honggou Formation, the best fit to the distinctive pattern recorded for this interval in the East Xining section (R1 to R3) is provided by C20r to C22r of the GPTS. This supports correlation in the Xiejia section of N19 in the upper member of the Honggou Formation to C20n and R18 in the lowermost part of the Mahalagou Formation to C18r-C19r. We note however some discrepancies between the East Xining and Xiejia magnetostratigraphic records (N20 of Xiejia absent in East Xining and N21 of Xiejia thinner than N2 in East Xining). These may be attributed to unidentified secondary magnetization component in sampled gypsum in the Xiejia section, insufficient sampling resolution in the East Xining section and/or slight differences in accumulation rates between the Xiejia and East Xining sections. In the lowermost part of the Xiejia section, N22-N23 are tentatively correlated to the C22n-C23n of the GPTS in agreement with Paleocene to Eocene fossils reported from the upper part of the Qiejiaochuan Formation.

[11] For the Xiejia Formation, above the distinctive C12r-C13n-C13r pattern, our correlation to the GPTS is based on the Xiejia section only and justified as follows. The thickest recorded normal polarity zone N11 is correlated to C9n with a reasonable fit below of C10n, C11n and C12n to zones N12, N13, and N14, respectively. Above C9n, we correlate C7n-C8n to zones N9-N10 (Figure 8). According to this correlation, the age of the Xiejia fauna found at the 632 m level in the reversed polarity zone R9 is bracketed between the limits of C7n and C7An (i.e., 25.183–25.496 Ma) which is sensibly older than the early Miocene age previously assigned to this fauna as will be discussed below. Above C6r and until the long normal C6n, the GPTS is characterized by dominantly reversed polarity with short normal intervals ranging from 34 to 324 kyr in duration. Although the sampling resolution in this part of the section is not sufficient to pick up exactly the pattern of these small chrons as shown by the estimated time intervals between levels (Table S1), the largest normal zone N4 recorded at the top of the Chetougou Formation is obviously correlated to C6n. Below, the normal zones N5, N6 and N7–N8 are tentatively correlated to the series of small normal chrons C6An, C6Bn and C6Cn, respectively. According to this correlation, the fossiliferous basal sandstone of the Chetougou Formation lies in the reverse zone between C6Bn.2n and C6Cn.1n (23.069–23.353 Ma). Above C6n and into the Xianshuihe Formation, N3 correlates nicely with C5En, and we further correlate N1 with C5Dn implying problems in the two samples recording N2.

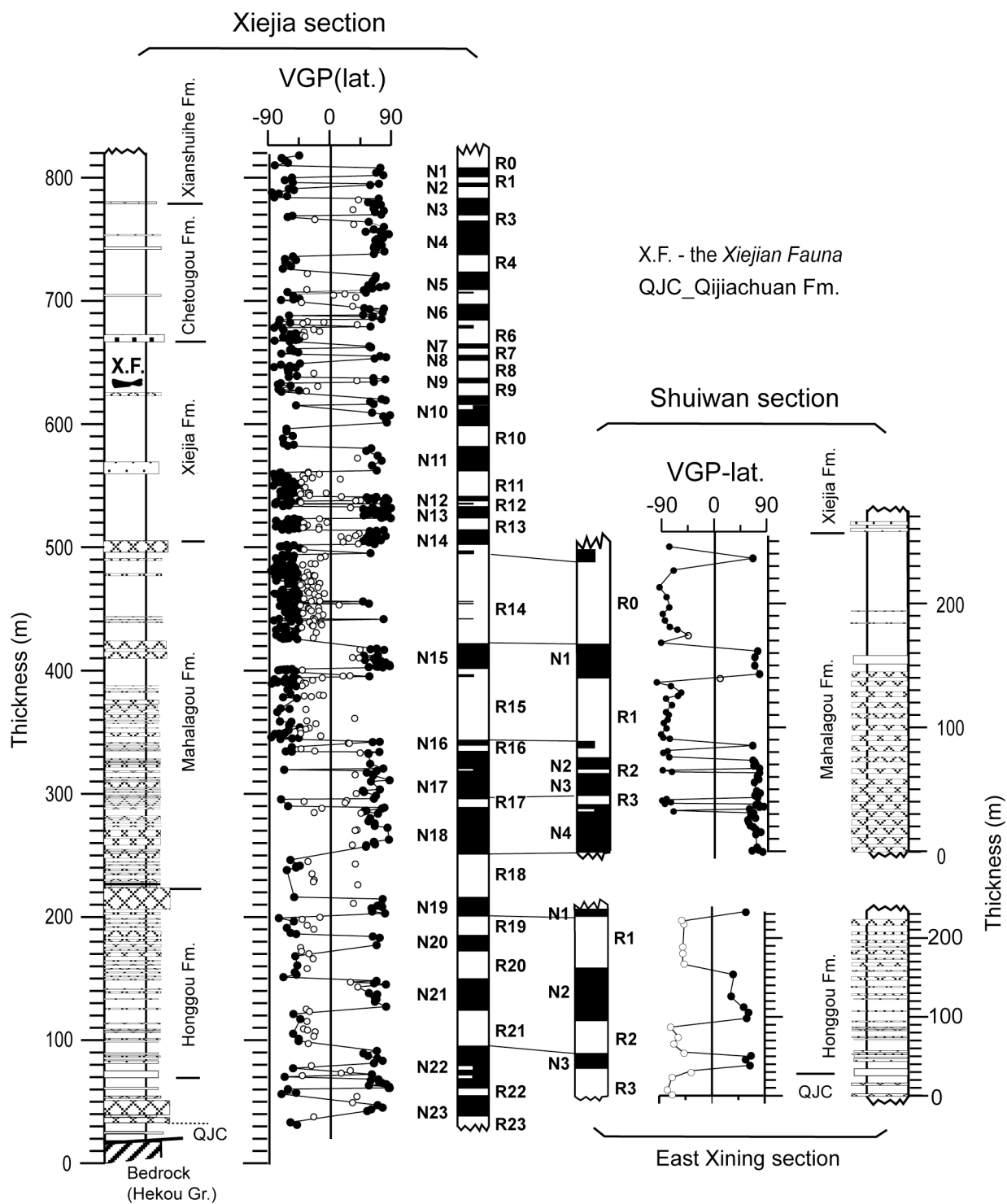


Figure 7. Observed stratigraphy and paleomagnetic polarity zones (black for normal and white for reversed) indicated by calculated latitude of virtual geomagnetic pole (VGP latitude) at the Xiejia (this study), Shuiwan (this study), and East Xining [Horton *et al.*, 2004] sections. VGP latitudes below 45° (white dots) have been discarded to determine polarity zones. Polarity zones defined by only one VGP latitude are depicted by half length zones.

4.2. Apparent Inconsistencies With Fossil Mammal Record

[12] In the Guide Group, our correlation implies older age assignments than previously proposed for the Xiejia, Chetougou and Xianshuihe formations based on early, middle

and middle to late Miocene fossil contents, respectively (Table 1 for a review). The Xiejia fauna contain fossils that are generally found in late Oligocene to early Miocene environments. It was initially assigned an early Miocene age possibly bracketed between mammal zones MN1 to MN4

(a) rejected correlations

(b) preferred correlations

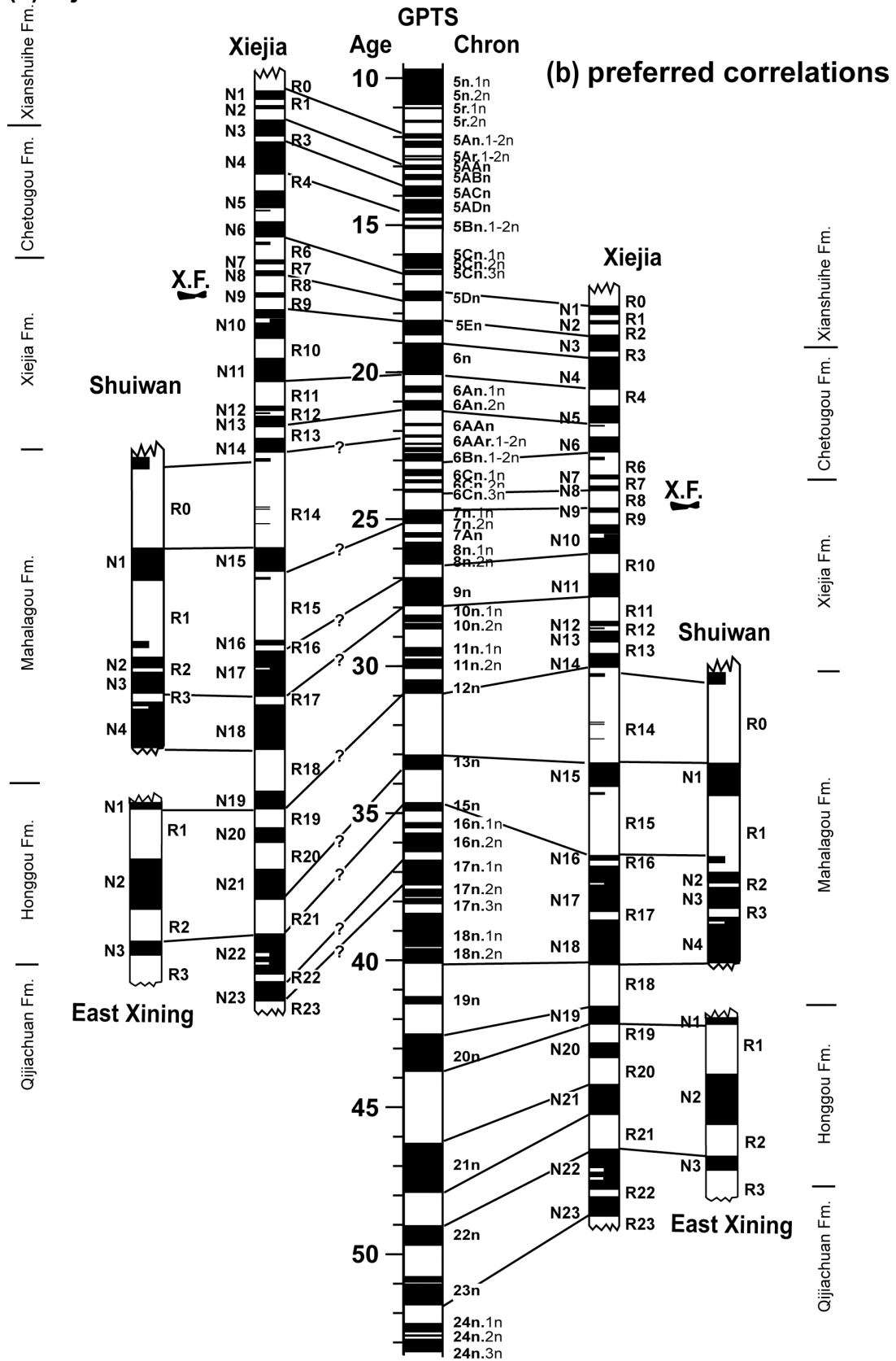


Figure 8. (b) Preferred and (a) rejected correlations of the observed polarity zones of the Xiejia, Shuiwan, and East Xining sections with the geomagnetic polarity timescale (GPTS) of *Cande and Kent* [1995].

(circa 23.8–15.8 Ma) because the principal elements of the assemblage demonstrates more derived features than the Taben Buluk fauna of presumed late Oligocene age and based on the similarity with Aquitanian to Burdigalian faunas of Europe [Li and Qiu, 1980; Li et al., 1981; Qiu et al., 1981]. However, based on more recent findings and comparison to other Chinese faunas constrained by radiometric dating (Sihong fauna at ~17 Ma and Shanwang fauna at ~18 Ma), an age older than 20 Ma, has been reassigned to the Xiejia fauna [Qiu et al., 1999; Qiu Z. and Qiu Z., personal communication, 2005]. Consistent with the latter, our results indicate latest Oligocene age (25.183–25.496 Ma) for the Xiejia fauna.

[13] Further up in the section, Li and Qiu [1980] report a fragment fossil (*Critecidae* ?cf. *Eumyarion* sp.) uncovered in the basal sandstone of the Chetougou Formation (667 m level) initially attributed a middle Miocene age (circa 16.4–11.2 Ma). However, this tentative age is inconsistent both with the 23.069–23.353 Ma age of this horizon according to our magnetostratigraphic correlation and with the older than 20 Ma age of the Xiejia fauna found only 45 m below and suggesting earliest Miocene age for the fragment.

[14] Furthermore, we argue that the apparent discrepancy between our magnetostratigraphic ages with the regional fossil occurrences lies in the difficulty to perform stratigraphic correlations in the Guide Group due to the lack of distinctive extensive marker beds. Formation boundaries for the Xiejia, Chetougou, and Xianshuihe formations are ambiguously defined by the occurrence of sandstone beds. These lenticular beds, often fossiliferous, reflect meandering channel deposits that are not laterally extensive in the stratigraphy. For example, the above mentioned sandstone defining the base of the Chetougou Formation in the Xiejia section has a maximum thickness of 10 m thinning laterally into a submeter thick silty horizon that may be easily overlooked in the stratigraphy. For these reasons, inaccuracies in basin wide stratigraphic correlations of fossil localities based on lithologic distinctions in the Guide Group may explain the apparent discrepancy of the magnetostratigraphic age indication in the upper part of the Xiejia section with the correlated fossil records of the Chetougou and Xianshuihe formations.

[15] With regards to this discrepancy with the fossil record, we investigate the unlikelihood of a younger alternative to our preferred correlation to the GPTS. The next possible correlation of the long normal polarity zone N11 recorded in the Xiejia Formation is provided by the long normal interval C6n of the GPTS at circa 20 Ma (Figure 8a). This leads to the tentative correlation of polarity zones above N11 to chrons C5An1n to C5En as shown on the rejected correlation. Below N11 this rejected correlation could continue with N12, N13 to C6An.1n, C6An.2n, respectively. Below N13 however, correlation becomes virtually impossible as illustrated by evasive ties to the GPTS given on Figure 8a. Although this alternative correlation is in agreement with the presumed middle Miocene and middle to late Miocene ages of the Chetougou and Xianshuihe formations, respectively, we reject it as viable for the following reasons: (1) it does not provide a convincing correlation to the GPTS below N13 and especially it would imply that some significantly long normal chrons (such as C8n) have been missed in both parallel sections

above and below N1 at Shuiwan and N15 at Xiejia; (2) even above N13, its match to the pattern of the GPTS is inferior to that of our preferred correlation; (3) it would imply a significantly younger age (17.615–18.281 Ma) than the 20 Ma upper limit determined for the Xiejia fauna; and (4) it is in disagreement with the well-established Paleogene fossil record for the Xining Group formations. A remaining way to account for this alternative correlation and hence a younger age for the Guide Group formations, would be to allow important gaps in the stratigraphy. For example, combining our preferred correlation (Figure 8b) up to N13 with the rejected correlation (Figure 8a) from N13 upward would require that approximately 8 Myr are missing in the stratigraphic record. Alternatively, an unidentified paracomformity of over 5 Myr marked by the sandstone at the base of the Chetougou Formation would allow connecting our preferred correlation below C6Bn.1n at the reversed polarity zone R7, to the rejected correlation above C5Dn. Although the occurrence of hiatus in the record cannot be absolutely ruled out, we find very improbable that such large stratigraphic gaps would go by unnoticed and not be expressed by angular or at least erosional discordance; however the stratigraphy is, as stated above, concordant with continuous deposition of lacustrine mudstone disturbed only by a few lenticular sandstones (such as the basal sandstone of the Chetougou Formation) that are not laterally extensive and not exceeding 10 m in thickness.

4.3. Magnetostratigraphic Results

[16] Finally, when compared to alternative possibilities implying large stratigraphic discordance of which we found no geological evidence, our preferred correlation provides the best and simplest possible correlation to the GPTS of the observed paleomagnetic polarity patterns recorded at the Xiejia, Shuiwan, and East Xining sections. A jackknife technique [Tauxe and Gallet, 1991] was used to quantify the reliability of the observed magnetostratigraphy above. The obtained Jackknife parameters (J) have values of -0.2637 and -0.0867 in the Xiejia and Shuiwan sections, respectively, which fall within the range of 0 to -0.5 recommended for a robust magnetostratigraphic data set by [Tauxe and Gallet, 1991]. The J values predict that both sections have recovered more than 95% of the true number of polarity intervals (Figure 9). The depth versus age plot of the Xiejia section shows a first-order linear trend indicating principally constant accumulation rate at 2.2 cm/kyr average with low variation in the 1 to 5 cm/kyr range (Figure 10). This linear trend is in good agreement with our original assumption of low continuous sedimentary rate variations throughout the section. In detail, second-order accumulation rate variations outline a three-stage evolution with (1) constant lower rate (1.8 cm/kyr) from 52.0 Ma to 34.5 Ma; (2) highest rate (4.1 cm/kyr) during a comparatively shorter period (34.5–31.0 Ma); and (3) constant higher rate (2.3 cm/kyr) from 31.0 to 17.0 Ma (Table S3). These second-order variations are consistent with an apparent depositional environment change between the Xining and the Guide Groups marked by the disappearance of cyclic gypsum deposits between the middle member and the upper member of the Mahalagou Formation.

[17] According to our preferred correlation the age of the Xining basin stratigraphy can be constrained as follows. The

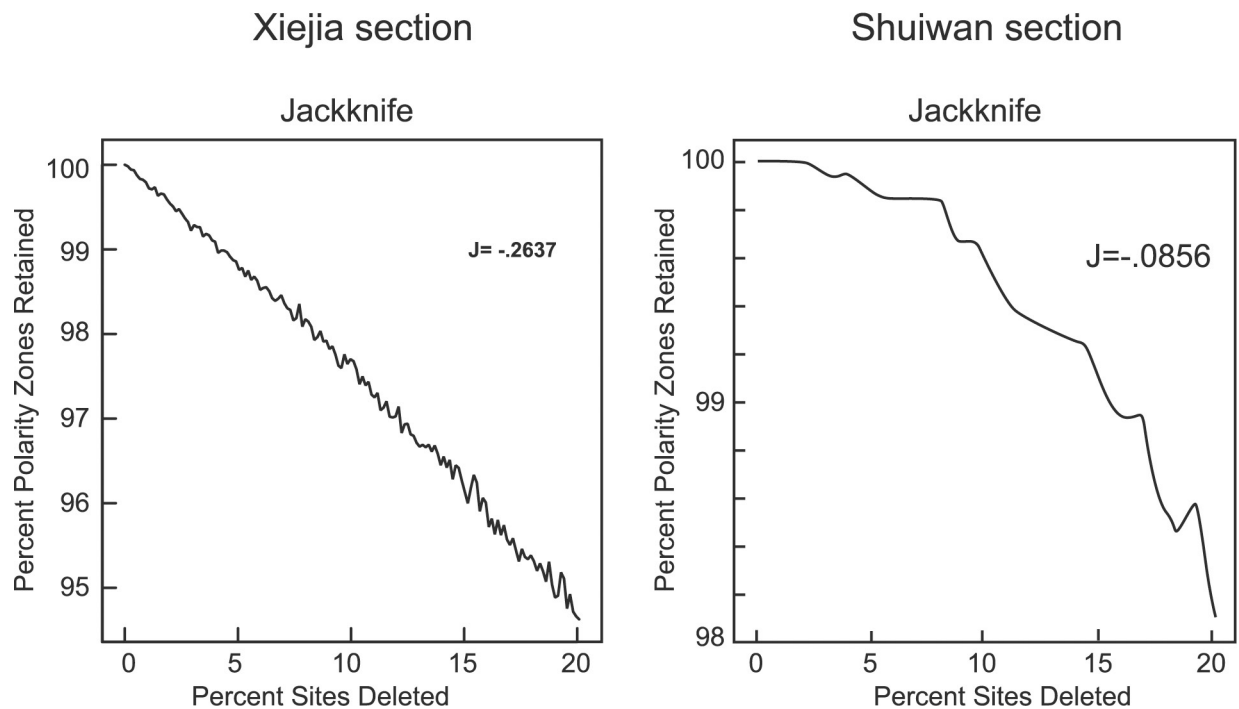


Figure 9. Magnetostratigraphic Jackknife analyses [Tauxe and Gallet, 1991] for the Xiejia and Shuiwan sections. The plot indicates the relationship between average percent of polarity zones retained and the percentage of sampling sites deleted, where the slope J is directly related to the robustness of the results. The obtained slopes J have values predicts that the sections have recovered more than 95% of the true number of polarity intervals.

base of the sampled stratigraphy is estimated at 52.0 Ma in the middle member of the Qijiachuan Formation. Extrapolating down an additional 10 to 60 m of stratigraphy of the lower Qijiachuan Formation (Table 1) at 1.8 cm/kyr accumulation rate estimated for the Xining Group, suggests initiation of deposition in the Xining basin between circa 52.5 and 55.0 Ma. Formation boundaries for the Honggou and Mahalagou are estimated at 50.0–41.5 Ma and 41.5–30.0 Ma, respectively. Within the Guide Group, formation boundaries for the Xiejia and Chetougou are estimated at 30.0–23.0 Ma and 23.0–18.0 Ma, respectively, with the Xiejia fauna bracketed between 25.183 and 25.496 Ma. The base of the Xianshuihe Formation is further indicated at 18.0 Ma but our sampling stops at an estimated 17.0 Ma before the top of this formation which is not exposed in the sampled section. When exposed in the Xining basin, the top of the Xianshuihe Formation is reported to be unconformably overlain by the late Miocene “diluvial deposits” of the Linxia Group [Qinghai Bureau of Geology and Mineral Resources, 1985, 1991] such that it is not possible in the Xining basin to estimate the original thickness of the Xianshuihe Formation.

5. Tectonic Implications

[18] On the basis of the sediment accumulation history constrained by our magnetostratigraphy of the Xining subbasin tied to biostratigraphic, sedimentologic, and structural data from the regional Cenozoic Longzhong basin we can address several issues concerning the tectonic evolution of the northeastern Tibetan Plateau. The most striking

outcome of this study is the nearly constant and very low accumulation rates from ~55.0 to 17.0 Ma recorded in the Xining basin at the margin of the present-day Tibetan Plateau. We interpret this result to indicate that no major regional tectonic event implying large sediment accumulation variations has affected the Xining basin deposition during this considerable time window. In contrast, large variations in depositional environment before and after deposition of the studied sediments suggest important tectonic activity after 17.0 Ma and during basin initiation at circa 55.0–52.5 Ma. As discussed below, the second-order variations within the accumulation record (change from lower to slightly higher rates after a transitional period circa 34.5 to 31.0 Ma) can be interpreted to result from either a distal tectonic event or to be of climatic origin. Before further considerations, it should be noted that due to a lack of independent evidence for surface elevation through time, the tectonic subsidence cannot be absolutely estimated and sediment accumulation need not be directly attributed to subsidence (particularly in topographically closed basins [Metivier *et al.*, 1998]). However, we assume that these subsidence considerations can be avoided by correlating the first-order accumulation variations in the Xining basin to independent geological constraints available in the region in order to put forward tectonic implications discussed below.

5.1. Paleocene–Early Eocene Basin Initiation (Circa 55.0–52.5 Ma)

[19] The onset of deposition in the Xining basin estimated at 52.5–55.0 Ma correlates well with the documented history of other Tibetan basins. Initiation of the nearby

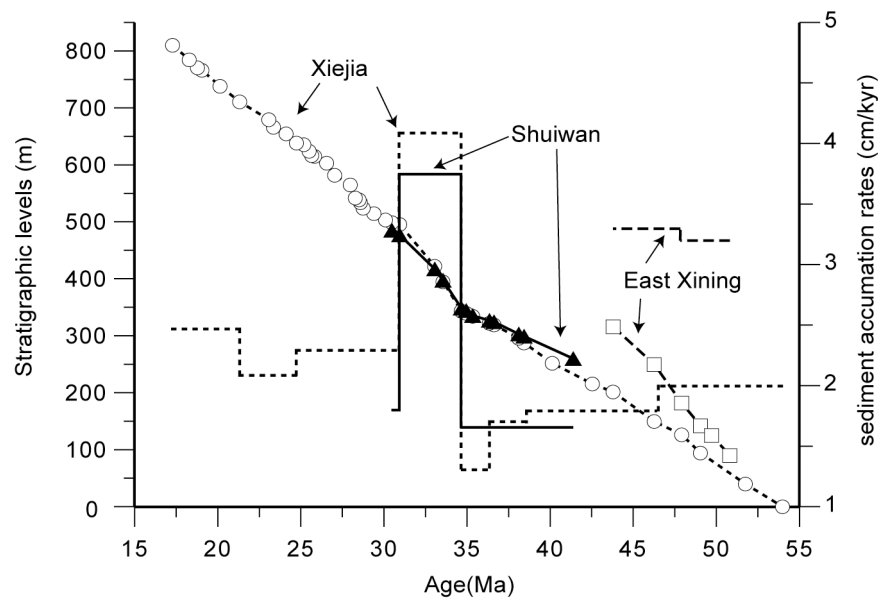


Figure 10. Stratigraphic level (strat level) in meters versus age according to our preferred magnetostratigraphic correlation to the GPTS at the Xiejia (circles) and Shuiwan (triangles) and East Xining (squares) sections. Dashed lines indicate sediment accumulation rates calculated from the sediment thickness between limits of correlated chrons in circa 3 Ma windows (see Table S3 for detailed rate calculations).

Lanzhou subbasin of the Cenozoic Longzhong basin is indicated by uncomformable deposition of coarse sandstone of the Xiliugou Formation with biostratigraphic and magnetostratigraphic age control at circa 58 Ma [Qiu *et al.*, 2001; Yue *et al.*, 2001a]. In the Nangqian-Yushu region of east central Tibet, initiation of the Shanglaxiu basin is recorded by Paleogene fossil bearing syncontractional strata covered by lower Eocene (51–49 Ma) igneous rocks post-dating the northeast-southwest contraction [Horton *et al.*, 2003; Spurlin *et al.*, 2005]. In north central Tibet along the Jinsha suture zone, initiation of the Hoh Xil basin is estimated at 56–51 Ma through magnetostratigraphic analysis of the Fenguoshan Group [Liu *et al.*, 2001, 2003]. In the Qaidam basin, the onset of subsidence is documented by the deposition of basal conglomeratic units of the Paleogene Lulehe Formation prior to 46–49 Ma [Qinghai Bureau of Geology and Mineral Resources, 1991; Yin *et al.*, 2002]. The driving mechanism for this Paleocene–early Eocene basin initiation in the northern Tibetan Plateau has been tentatively interpreted to result from early and far-field effect of the Indo-Asia collision [Horton *et al.*, 2003; Spurlin *et al.*, 2005; Wang *et al.*, 2002; Yin *et al.*, 2002]. While this view is consistent with the observed northeast-southwest contraction in the Shanglaxiu basin [Spurlin *et al.*, 2005], the definite tectonic setting of the early Xining basin remains to be constrained by structural and thermo-chronologic information on its initial bounding structure.

5.2. Eocene/Oligocene Depositional Transition (34.5–31.0 Ma)

[20] In the Xining basin, the Paleocene–early Eocene basin initiation is followed by low constant accumulation (1.8 cm/kyr) of gypsiferous lacustrine successions until a transition to different depositional environment. This transition is expressed by progressive fading of cyclic gypsum

beds and an increase in sedimentary rates (4.1 cm/kyr) between 34.5 and 31.0 Ma. This transition period is followed by constant continuous accumulation (2.3 cm/kyr) of the formations of the Guide Groups. Several observations suggest that this change affected at least the entire 100,000 km² of the Longzhong basin. Several hundred kilometers to the east of the Xining basin, we observed the identical distinct facies transition at the Duittingou section in the Lanzhou basin where a change of accumulation rate from 2.5 cm/kyr to 3.8 cm/kyr is reported in the same age window [Qiu *et al.*, 2001; Yue *et al.*, 2001a]. The Eocene/Oligocene depositional transition observed in the Xining basin may be correlated to initiation of the Linxia basin reported to occur before 29 Ma in a thrust-related flexural subsidence setting [Fang *et al.*, 2003]. In addition, tectonic rotations and exhumation ages have been reported regionally in this general age range supporting that this depositional transition may be related to an important tectonic event [Dupont-Nivet *et al.*, 2004; Jolivet *et al.*, 2002; Mock *et al.*, 1999]. In the Xining basin however, the transition is not manifested by an unconformity of any sort, appearance of proximal deposits, coarsening upward sequences or drastic change in accumulation rate, as would be expected if related to the activation of nearby bounding structures (e.g., Laji Shan fault, Haiyan fault, North middle Qilian Shan fault). Thus we argue that a tectonic source accounting for the slight sediment accumulation variation observed at the Eocene/Oligocene depositional transition would have to be comparatively distal from the Xining basin. Finally, it should be noted that a climatic driver for the observed transition cannot be ruled out. In favor of this suggestion are (1) the observed change of depositional environment and (2) the fact that the age window (34.5–31.0 Ma) comprises the Eocene-Oligocene boundary

(33.7 Ma) marked by a drastic global climate change [Zachos *et al.*, 2001].

5.3. Middle to Late Miocene Basin Disruption (Post-17 Ma)

[21] Our record of the continuous constant accumulation (2.3 cm/kyr) of the Guide Group series finishes at an estimated 17.0 Ma at the top of the Xiejia section yielding a maximum age for the end of this depositional system. Folding and faulting involving the Guide Formation are found within the NNE trending Xining, Pingan, and Ledu anticlines as well as along the Laji Shan and Haiyan faults indicating that these structures have been active after deposition of the Guide Group (i.e., after 17 Ma). In the Xining basin, the Guide Group is reported to be unconformably overlain by the conglomeratic Linxia Group bearing late Miocene fossils (Table 1) suggesting that an important event starting in middle to late Miocene time disrupted basin deposition. These observations together suggest that most of the tectonic activity occurred after 17 Ma in the Xining basin and strong deformation and uplift may have continued to the present, resulting in continuous incision of the basin forming the geomorphologic features observed today. To the east of the Xining basin, a similar setting is documented in the Lanzhou basin where the top of the exposed Guide Group is dated at circa 15 Ma [Qiu *et al.*, 2001]. In the Guide-Gonghe basin to the south, Fang *et al.* [Fang *et al.*, 2005] document middle Miocene sediments with low accumulation rates overlain by a coarsening upward gravelly sequence, characterized by distinctly higher accumulation rates (20–200 cm/kyr) from circa 11.5 to 1.8 Ma (see also Pares *et al.* [2003]). Throughout the Qaidam basin and Qilian Shan–Nan Shan ranges to the west, numerous studies report similar late Miocene to Pliocene increased sediment accumulation documented by a rich mammal biostratigraphic record and magnetostratigraphic correlations [Gilder *et al.*, 2001; Metivier *et al.*, 1998; Sun *et al.*, 2005; Wang *et al.*, 2003; Yin *et al.*, 2002]. This well documented late Miocene to Pliocene increased tectonic activity in northeastern Tibet supports northeastward stepwise uplift of the Tibetan Plateau proposed by Tapponnier *et al.* [2001]. In addition, the observed drastic accumulation rate increase are consistent with tectonic mechanisms of fault induced closure of drainage basin outlets [e.g., Metivier *et al.*, 1998; Sobel *et al.*, 2003] as exemplified by late Miocene compartmentalization of the >100,000 km² Longzhong basin into <30,000 km² basins such as the Xining basin by compressional and transpressional range [Horton *et al.*, 2004; Meyer *et al.*, 1998].

6. Conclusions

[22] The preceding magnetostratigraphic analysis of Cenozoic sediments from the Xining basin provides new insight on the timing and character of deformation in the northeastern Tibetan Plateau region during the development of the Indo-Asia continental collision. Like other basins of that region, the Xining Basin evolution is characterized by continuously low sediment accumulation rates (1–10 cm/kyr) during Eocene to middle Miocene time. The age correlation indicates principally constant accumulation rate (average 2.2 cm/kyr) throughout the section from

52.0 Ma to 17.0 Ma. We interpret this result to indicate that no nearby major tectonic event affected basin deposition during this time span. In detail, minor accumulation rate variations between 34.5 and 31.0 Ma may record the effect of distant tectonic activity or a change of depositional environment due to climatic variations. More importantly, the early Eocene basin initiation implied by our results is coeval with initiation of other basins throughout the northern Tibetan region. However, most of the tectonic activity experienced by this region occurred after the end of our stratigraphic record at 17 Ma in agreement with existing geological constraints and tectonic models. Our results provide improved age control on the well-documented rich biostratigraphic content of the Xining basin, including the age of the Xiejia mammal fauna bracketed between 25.183 and 25.496 Ma.

[23] **Acknowledgments.** Reviews by R. Enkin, Y. Chen, and an anonymous reviewer significantly improved the submitted manuscript. We thank Zhu Rixiang and Mark Dekkers for laboratory assistance and Xu Xianhai and Gao Donglin for field assistance. We thank Qiu Zhanxiang, Qiu Zhuding, and Hans de Bruijn for benefic discussions about vertebrate paleontology. This work was cosupported by the Chinese NSFC funds (40334038, 40421101, 40571017), National Basic Research Program of China (2005CB422001), CAS President fund, European Union Marie Curie Fellowship and Netherlands Science Organisation (NWO) grants for G. Dupont-Nivet, S. Dai, and C. Song.

References

- Cande, S. C., and D. V. Kent (1995), Revised calibration of the geomagnetic polarity timescale for the Late Cretaceous and Cenozoic, *J. Geophys. Res.*, **100**, 6093–6095.
- de Boer, C. B., and M. J. Dekkers (1996), Grain-size dependence of the rock magnetic properties for a natural maghemite, *Geophys. Res. Lett.*, **23**, 2815–2818.
- Delville, N., N. Arnaud, and J. M. Montel (2001), Paleozoic to Cenozoic deformation along Altyn-Tagh fault in the Altyn Shan massif area, eastern Qilian Shan, northeast Tibet, China, in *Paleozoic and Mesozoic Tectonic Evolution of Central and Eastern Asia: From Continental Assembly to Intracontinental Deformation*, edited by M. S. Hendrix and G. A. Davis, *Mem. Geol. Soc. Am.*, **194**, 269–292.
- Dettman, D. L., X. Fang, C. N. Garzzone, and J. Li (2003), Uplift-driven climate change at 12 Ma: A long small delta, d18O record from the NE margin of the Tibetan plateau, *Earth Planet. Sci. Lett.*, **214**, 267–277.
- Dupont-Nivet, G., R. F. Butler, A. Yin, D. Robinson, Y. Zhang, W. S. Qiao, and J. Melosh (2004), Concentration of crustal displacement along a weak Altyn Tagh fault: Evidence from paleomagnetism of the northern Tibetan Plateau, *Tectonics*, **23**, TC1020, doi:10.1029/2002TC001397.
- Fang, X., C. Garzzone, R. Van der Voo, J. Li, and M. Fan (2003), Flexural subsidence by 29 Ma on the NE edge of Tibet from the magnetostratigraphy of Linxia Basin, China, *Earth Planet. Sci. Lett.*, **210**(3–4), 545–560.
- Fang, X., Z. Zhao, J. Li, M. Yan, B. Pan, C. Song, and S. Dai (2004), Late Cenozoic magnetostratigraphy of Laojunmiao anticlines of northern Qilian shan (Mts.) and its implications for uplift of northern Tibetan Plateau (in Chinese), *Sci. China, Ser. D*, **32**(2), 97–106.
- Fang, X., M. Yan, R. Van der Voo, D. K. Rea, C. Song, J. M. Pares, J. Gao, J. Nie, and S. Dai (2005), Late Cenozoic deformation and uplift of the NE Tibetan Plateau: Evidence from high-resolution magnetostratigraphy of the Guide Basin, Qinghai Province, China, *Geol. Soc. Am. Bull.*, **117**, 1208–1225, doi:10.1130/B25727.1.
- Flynn, L. J., W. Downs, N. D. Opdyke, K. Huang, E. Lindsay, J. Ye, G. Xie, and X. Wang (1999), Recent advances in the small mammal biostratigraphy and magnetostratigraphy of Lanzhou Basin, *Chin. Sci. Bull.*, **44**, Suppl. 1, 109–117.
- Garzzone, C., M. J. Ikari, and A. R. Basu (2005), Source of Oligocene to Pliocene sedimentary rocks in the Linxia basin in northeastern Tibet from Nd isotopes: Implications for tectonic forcing of climate, *Geol. Soc. Am. Bull.*, **117**(9), 1156–1166, doi:10.1130/B25743.1.
- George, A. D., S. J. Marshallsea, K.-H. Wyrwoll, J. Chen, and Y. Lu (2001), Miocene cooling in the Northern Qilian Shan, northeastern margin of the Tibetan Plateau, revealed by apatite fission-track and vitrinite-reflectance analysis, *Geology*, **29**(10), 939–942.

- Gilder, S., Y. Chen, and S. Sen (2001), Oligo-Miocene magnetostratigraphy and rock magnetism of the Xishuigou section, Subei (Gansu Province, western China) and implications for shallow inclinations in central Asia, *J. Geophys. Res.*, *106*(B12), 30,505–30,522.
- Hao, Y. C. (1988), Cretaceous and Palaeogene ostracod biostratigraphy in Xining and Minhe basins of China, in *Evolutionary Biology of Ostracoda*, edited by T. Hanai, N. Ikeya, and K. Ishizaki, pp. 1163–1171, Elsevier, New York.
- He, J. D., D. S. Van Nieuwenhuise, and F. M. Swain (1988), Biostratigraphy, i. E. of Paleogene non-marine Ostracoda from east China, and e. b. Biology of Ostracoda, Biostratigraphy of Paleogene non-marine Ostracoda from east China, in *Evolutionary Biology of Ostracoda*, edited by T. Hanai, N. Ikeya, and K. Ishizaki, pp. 1153–1161, Elsevier, New York.
- Horton, B. K., A. Yin, M. S. Spurlin, J. Zhou, and J. Wang (2003), Paleocene-Eocene syncontractional sedimentation in narrow, lacustrine-dominated basins of east-central Tibet, *Geol. Soc. Am. Bull.*, *114*(7), 771–786.
- Horton, B. K., G. Dupont-Nivet, J. Zhou, G. L. Waanders, R. F. Butler, and J. Wang (2004), Mesozoic-Cenozoic evolution of the Xining-Minhe and Dangchang basins, northeastern Tibetan Plateau: Magnetostratigraphic and biostratigraphic results, *J. Geophys. Res.*, *109*, B04402, doi:10.1029/2003JB002913.
- Houseman, G., and P. England (1996), A lithospheric-thickening model for the Indo-Asian collision, in *World and Regional Geology Series*, edited by A. Yin and T. M. Harrison, pp. 3–17, Cambridge Univ. Press, New York.
- Jolivet, M., M. Brunel, D. Seward, Z. Xu, J. Yang, F. Roger, P. Tapponnier, J. Malavieille, N. Arnaud, and C. Wu (2002), Mesozoic and Cenozoic tectonics of the northern edge of the Tibetan Plateau: Fission-track constraints, *Tectonophysics*, *343*(1–2), 111–134.
- Kirschvink, J. L. (1980), The least-square line and plane and the analysis of paleomagnetic data, *Geophys. J. R. Astron. Soc.*, *62*, 699–718.
- Li, C., and Z. Qiu (1980), Early Miocene mammalian fossils of Xining Basin, Qinghai, *Vertebrata Palasiatica*, *18*(3), 198–214.
- Li, C., Z. Qiu, and S. Wang (1981), Discussion on Miocene stratigraphy and mammals from Xining basin, *Qinghai, Vertebrata Palasiatica*, *19*(4), 313–320.
- Li, H. J., Z. Yang, Z. Xu, C. Wu, Y. Wang, R. Shi, and J. G. Liou (2002), Geological and chronological evidence of Indo-Chinese strike-slip movement in the Altyn Tagh fault zone (in Chinese), *Chin. Sci. Bull.*, *47*(1), 27–32.
- Li, J. (1995), *Uplift of Qinghai-Xizang (Tibet) Plateau and Global Change*, pp. 210, Lanzhou Univ. Press, Lanzhou, China.
- Li, J., X. Fang, R. Van der Voo, J. Z. Zhu, C. MacNiocail, J. Cao, W. Zhong, H. Chen, J. Wang, and Y. Zhang (1997), Late Cenozoic magnetostratigraphy (11–0 Ma) of the Dongshanding and Wangjiashan sections in the Longzhong Basin, western China, *Geol. Mijbouw*, *76*, 121–134.
- Liu, G., and R. Yang (1999), Pollen assemblages of the late Eocene Nadu Formation from the Bose basin of Guangxi, southern China, *Palynology*, *23*, 97–114.
- Liu, J., P. H., X. Ge, S. Ren, Y. Liu, and H. Ye (2001), An early faulting along the Altun Mountains, NW China, *Z. Dtsch. Geol. Ges.*, *152*, 379–386.
- Liu, Z., X. Zhao, C. Wang, S. Liu, and H. Yi (2003), Magnetostratigraphy of Tertiary sediments from the Hoh Xil Basin: Implications for the Cenozoic history of the Tibetan Plateau, *Geophys. J. Int.*, *154*, 233–252.
- Lowrie, W. (1990), Identification of ferromagnetic minerals in a rock by coercivity and unblocking temperature properties, *Geophys. Res. Lett.*, *17*, 159–162.
- Meng, Q.-R., J.-M. Hu, and F.-Z. Yang (2001), Timing and magnitude of displacement on the Altyn Tagh fault: Constraints from stratigraphic correlation of adjoining Tarim and Qaidam basins, NW China, *Terra Nova*, *13*(2), 86–91.
- Metivier, F., Y. Gaudemer, P. Tapponnier, and B. Meyer (1998), North-eastward growth of the Tibet plateau deduced from balanced reconstruction of two depositional areas: The Qaidam and Hexi corridor basins, China, *Tectonics*, *17*, 823–842.
- Meyer, B., P. Tapponnier, L. Bourjot, F. Metivier, Y. Gaudemer, G. Peltzer, G. Shummin, and C. Zhitai (1998), Crustal thickening in the Gansu-Qinghai, lithospheric mantle, oblique and strike-slip controlled growth of the Tibetan Plateau, *Geophys. J. Int.*, *135*, 1–47.
- Mock, C., N. Arnaud, and J.-M. Cantagrel (1999), An early unroofing in northeastern Tibet? Constraints from $^{40}\text{Ar}/^{39}\text{Ar}$ thermochronology on granitoids from the eastern Kunlun range (Qinghai, NW China), *Earth Planet. Sci. Lett.*, *171*, 107–122.
- Molnar, P., P. England, and J. Martinod (1993), Mantle dynamics, uplift of the Tibetan Plateau, and the Indian monsoon, *Rev. Geophys.*, *31*(4), 357–396.
- Pares, J. M., R. Van der Voo, W. R. Downs, M. Yan, and X. Fang (2003), Northeastward growth and uplift of the Tibetan Plateau: Magnetostratigraphic insights from the Guide Basin, *J. Geophys. Res.*, *108*(B1), 2017, doi:10.1029/2001JB001349.
- Qinghai Bureau of Geology and Mineral Resources (1985), Geologic maps of the Duoba, Gaodian, Tianjiagai, and Xining regions, 4 sheets, with regional geologic report (1:50,000 scale), 199 pp., Geol. Publ. House, Beijing.
- Qinghai Bureau of Geology and Mineral Resources (1991), *Regional Geology of the Qinghai Province*, 662 pp., Geol. Publ. House, Beijing.
- Qiu, Z., C. Li, and S. Wang (1981), Miocene mammals fossils from Xining Basin, Qinghai, *Vertebrata Palasiatica*, *19*(2), 156–173.
- Qiu, Z., W. Wu, and Z. Qiu (1999), Miocene mammal faunal sequence of China: Paleozoogeography and Eurasian relationships, in *The Miocene Land Mammals of Europe*, edited by G. Rossner and K. Heissig, pp. 443–455, F. Pfeil, Munich, Germany.
- Qiu, Z., B. Wang, Z. Qiu, F. Heller, L. Yue, G. Xie, and X. Wang (2001), Land-mammal geochronology and magnetostratigraphy of mid-Tertiary deposits in the Lanzhou Basin, Gansu Province, China, *Eclogae Geol. Helv.*, *94*, 373–385.
- Ritts, B. D., and U. Biffi (2000), Magnitude of post-Middle Jurassic (Bajocian) displacement on the central Altyn Tagh fault system, north-west China, *Geol. Soc. Am. Bull.*, *112*, 61–74.
- Sobel, E. R., N. Arnaud, M. Jolivet, B. D. Ritts, and M. Brunel (2001), Jurassic to Cenozoic exhumation history of the Altyn Tagh Range, northwest China, constrained by $^{40}\text{Ar}/^{39}\text{Ar}$ and apatite fission track thermochronology, in *Paleozoic and Mesozoic Tectonic Evolution of Central Asia: From Continental Assembly to Intracontinental Deformation, Paleozoic and Mesozoic Tectonic Evolution of Central and Eastern Asia: From Continental Assembly to Intracontinental Deformation*, edited by M. S. Hendrix and G. A. Davis, *Mem. Geol. Soc. Am.*, *194*, 247–267.
- Sobel, E. R., G. E. Hilley, and M. R. Strecker (2003), Formation of internally drained contractional basins by aridity-limited bedrock incision, *J. Geophys. Res.*, *108*(B7), 2344, doi:10.1029/2002JB001883.
- Spurlin, M. S., A. Yin, B. K. Horton, J. Zhou, and J. Wang (2005), Structural evolution of the Yushu-Nangqian region and its relationship to syncontractional igneous activity, east-central Tibet, *Geol. Soc. Am. Bull.*, *117*, 1293–1317, doi:10.1130/B25572.1.
- Sun, J. M., R. X. Zhu, and Z. S. An (2005), Tectonic uplift in the northern Tibetan Plateau since 13.7 Ma ago inferred from molasse deposits along the Altyn Tagh Fault, *Earth Planet. Sci. Lett.*, *235*, 641–653, doi:10.1016/j.epsl.2005.04.034.
- Sun, X., Y. Zhao, and Z. He (1984), The Oligocene-Miocene palynological assemblages from the Xining-Minhe basin (in Chinese with English abstract), *Geol. Rev.*, *30*(3), 207–216.
- Tapponnier, P., et al. (1990), Active thrusting and folding in the Qilian Shan, and decoupling between upper crust and mantle in northeastern Tibet, *Earth Planet. Sci. Lett.*, *97*, 382–403.
- Tapponnier, P., Z. Xu, F. Roger, B. Meyer, N. Arnaud, G. Wittlinger, and J. Yang (2001), Oblique stepwise rise and growth of the Tibetan Plateau, *Science*, *294*, 1671–1677.
- Tauxe, L. (1998), *Paleomagnetic Principles and Practice*, 299 pp., Springer, New York.
- Tauxe, L., and C. Badgley (1988), Stratigraphy and remanence acquisition of a paleomagnetic reversal in alluvial Siwalik rocks of Pakistan, *Sedimentology*, *35*, 697–715.
- Tauxe, L., and Y. Gallet (1991), A jackknife for magnetostratigraphy, *Geophys. Res. Lett.*, *18*, 1783–1786.
- Wang, C., Z. Liu, H. Yi, S. Liu, and X. Zhao (2002), Tertiary crustal shortening and peneplanation in the Hoh Xil region: Implications for the tectonic history of the northern Tibetan Plateau, *J. Asian Earth Sci.*, *20*(3), 211–223.
- Wang, D.-N., X.-Y. Sun, and Y.-N. Zhao (1990), Late Cretaceous to Tertiary palynofloras in Xinjiang and Qinghai, China, *Rev. Palaeobot. Palynol.*, *65*(1–4), 95–104.
- Wang, E. (1997), Displacement and timing along the northern trend of the Altyn Tagh fault zone, Northern Tibet, *Earth Planet. Sci. Lett.*, *150*, 55–64.
- Wang, X., B. Wang, Z. Qiu, G. Xie, J. Xie, W. Downs, Z. Qiu, and T. Deng (2003), Danghe area (western Gansu, China) biostratigraphy and implications for depositional history and tectonics of northern Tibetan Plateau, *Earth Planet. Sci. Lett.*, *208*(3–4), 253–269.
- Yin, A., and M. T. Harrison (2000), Geologic evolution of the Himalayan-Tibetan orogen, *Annu. Rev. Earth Planet. Sci.*, *28*, 211–280.
- Yin, A., et al. (2002), Tectonic history of the Altyn Tagh fault system in northern Tibet inferred from Cenozoic sedimentation, *Geol. Soc. Am. Bull.*, *114*(10), 1257–1295.
- Yu, J., H. Zhang, Q. Lin, Y. Gu, and Z. Z. Zhang (2003), Geological implications of Sporopollenites Flora from Tertiary Xining Group in Minhe County, Qinghai Province (in Chinese with English abstract), *Earth Sci. J. China Univ. Geosci.*, *28*(4), 401–405.

- Yu, Q., C. Li, F. Gu, Y. Hou, and K. Zhang (2001), *Regional Geologic Character and Field Mapping in the Northeast Margin of Qinghai-Tibet Plateau in Cenozoic* (in Chinese), 123 pp., China Univ. of Geosci. Press, Wuhan.
- Yue, L., F. Heller, Z. Qui, L. Zhang, G. Xie, Z. Qiu, and Y. Zhang (2001a), Magnetostratigraphy and paleoenvironmental record of Tertiary deposits of Lanzhou Basin, *Chin. Sci. Bull.*, 46(770–774).
- Yue, Y., B. D. Ritts, and S. A. Graham (2001b), Initiation and long-term slip history of the Altyn Tagh fault, *Int. Geol. Rev.*, 43, 1087–1093.
- Yue, Y., B. D. Ritts, S. A. Graham, J. L. Wooden, G. E. Gehrels, and Z. Zhang (2004), Slowing extrusion tectonics: Lowered estimate of post-Early Miocene slip rate for the Altyn Tagh fault, *Earth Planet. Sci. Lett.*, 217(1–2), 111–122.
- Zachos, J., M. Pagani, L. Sloan, E. Thomas, and K. Billups (2001), Trends, rhythms, and aberrations in global climate 65 Ma to present, *Science*, 292(5517), 686–693.
- Zhai, Y., and T. Cai (1984), The Tertiary system of Gansu province, in *Gansu Geology*, pp. 1–40, People's Press of Gansu, Gansu, China.
-
- S. Dai, J. Gao, C. Song, and W. Zhang, Key Laboratory of Western China's Environmental Systems, Lanzhou University, No. 222, Tianshui South Road, Lanzhou, 730000 China.
- G. Dupont-Nivet and W. Krijgsman, Faculty of Earth Sciences, Paleomagnetic Laboratory Fort Hoofddijk, Utrecht University, Budapestlaan 17, Utrecht, NL-3584 CD Netherlands.
- X. Fang, Institute of Tibetan Plateau Research, Chinese Academy of Sciences, No. 222, Tianshui South Road, Beijing, 100085 China. (fangxm@itpcas.ac.cn)
- C. Langereis, Faculty of Earth Sciences, Utrecht University, Budapestlaan 4, Utrecht, NL-3508 TA Netherlands.